Physics

Physics Research Publications

Purdue University *Year* 2008

Study of the semileptonic charm decays D-0 ->pi(-)e(+)nu e, D+->pi(0)e(+)nu e, D-0 -> K(-)e(+)nu e, and D+->(K)over-bar(0)e(+)nu e

S. Dobbs, Z. Metreveli, K. K. Seth, A. Tomaradze, J. Ernst, H. Severini, S. A. Dytman, W. Love, V. Savinov, O. Aquines, Z. Li, A. Lopez, S. Mehrabyan, H. Mendez, J. Ramirez, G. S. Huang, D. H. Miller, V. Pavlunin, B. Sanghi, I. P. J. Shipsey, B. Xin, G. S. Adams, M. Anderson, J. P. Cummings, I. Danko, J. Napolitano, Q. He, J. Insler, H. Muramatsu, C. S. Park, E. H. Thorndike, F. Yang, T. E. Coan, Y. S. Gao, F. Liu, M. Artuso, S. Blusk, J. Butt, J. Li, N. Menaa, R. Mountain, S. Nisar, K. Randrianarivony, R. Redjimi, R. Sia, T. Skwarnicki, S. Stone, J. C. Wang, K. Zhang, S. E. Csorna, G. Bonvicini, D. Cinabro, M. Dubrovin, A. Lincoln, D. M. Asner, K. W. Edwards, R. A. Briere, I. Brock, J. Chen, T. Ferguson, G. Tatishvili, H. Vogel, M. E. Watkins, J. L. Rosner, N. E. Adam, J. P. Alexander, K. Berkelman, D. G. Cassel, J. E. Duboscq, K. M. Ecklund, R. Ehrlich, L. Fields, L. Gibbons, R. Gray, S. W. Gray, D. L. Hartill, B. K. Heltsley, D. Hertz, C. D. Jones, J. Kandaswamy, D. L. Kreinick, V. E. Kuznetsov, H. Mahlke-Krueger, P. U. E. Onyisi, J. R. Patterson, D. Peterson, J. Pivarski, D. Riley, A. Ryd, A. J. Sadoff, H. Schwarthoff, X. Shi, S. Stroiney, W. M. Sun, T. Wilksen, M. Weinberger, S. B. Athar, R. Patel, V. Potlia, J. Yelton, P. Rubin, C. Cawlfield, B. I. Eisenstein, I. Karliner, D. Kim, N. Lowrey, P. Naik, C. Sedlack, M. Selen, E. J. White, J. Wiss, M. R. Shepherd, D. Besson, T. K. Pedlar, D. Cronin-Hennessy, K. Y. Gao, D. T. Gong, J. Hietala, Y. Kubota, T. Klein, B. W. Lang, R. Poling, A. W. Scott, A. Smith, and P. Zweber

Study of the semileptonic charm decays $D^0 \to \pi^- e^+ \nu_e$, $D^+ \to \pi^0 e^+ \nu_e$, $D^0 \to K^- e^+ \nu_e$, and $D^+ \to \bar{K}^0 e^+ \nu_e$

S. Dobbs,[1] Z. Metreveli,[1] K. K. Seth,[1] A. Tomaradze,[1] J. Ernst,[2] H. Severini,[3] S. A. Dytman,[4] W. Love,[4] V. Savinov,[4] O. Aquines,[5] Z. Li,[5] A. Lopez,[5] S. Mehrabyan,[5] H. Mendez,[5] J. Ramirez,[5] G. S. Huang,[6] D. H. Miller,[6] V. Pavlunin,[6] B. Sanghi,[6] I. P. J. Shipsey,[6] B. Xin,[6] G. S. Adams,[7] M. Anderson,[7] J. P. Cummings,[7] I. Danko,[7] J. Napolitano,[7] Q. He,[8] J. Insler,[8] H. Muramatsu,[8] C. S. Park,[8] E. H. Thorndike,[8] F. Yang,[8] T. E. Coan,[9] Y. S. Gao,[9] F. Liu,[9] M. Artuso,[10] S. Blusk,[10] J. Butt,[10] J. Li,[10] N. Menaa,[10] R. Mountain,[10] S. Nisar,[10] K. Randrianarivony,[10] R. Redjimi,[10] R. Sia,[10] T. Skwarnicki,[10] S. Stone,[10] J. C. Wang,[10] K. Zhang,[10] S. E. Csorna,[11] G. Bonvicini,[12] D. Cinabro,[12] M. Dubrovin,[12] A. Lincoln,[12] D. M. Asner,[13] K. W. Edwards,[13] R. A. Briere,[14] I. Brock,[14] J. Chen,[14] T. Ferguson,[14] G. Tatishvili,[14] H. Vogel,[14] M. E. Watkins,[14] J. L. Rosner,[15] N. E. Adam,[16] J. P. Alexander,[16] K. Berkelman,[16] D. G. Cassel,[16] J. E. Duboscq,[16] K. M. Ecklund,[16] R. Ehrlich,[16] L. Fields,[16] L. Gibbons,[16] R. Gray,[16] S. W. Gray,[16] D. L. Hartill,[16] B. K. Heltsley,[16] D. Hertz,[16] C. D. Jones,[16] J. Kandaswamy,[16] D. L. Kreinick,[16] V. E. Kuznetsov,[16] H. Mahlke-Krüger,[16] P. U. E. Onyisi,[16] J. R. Patterson,[16] D. Peterson,[16] J. Pivarski,[16] D. Riley,[16] A. Ryd,[16] A. J. Sadoff,[16] H. Schwarthoff,[16] X. Shi,[16] S. Stroiney,[16] W. M. Sun,[16] T. Wilksen,[16] M. Weinberger,[16] S. B. Athar,[17] R. Patel,[17] V. Potlia,[17] J. Yelton,[17] P. Rubin,[18] C. Cawlfield,[19] B. I. Eisenstein,[19] I. Karliner,[19] D. Kim,[19] N. Lowrey,[19] P. Naik,[19] C. Sedlack,[19] M. Selen,[19] E. J. White,[19] J. Wiss,[19] M. R. Shepherd,[20] D. Besson,[21] T. K. Pedlar,[22] D. Cronin-Hennessy,[23] K. Y. Gao,[23] D. T. Gong,[23] J. Hietala,[23] Y. Kubota,[23] T. Klein,[23] B. W. Lang,[23] R. Poling,[23] A. W. Scott,[23] A. Smith,[23] and P. Zweber[23]

(CLEO Collaboration)

[1]*Northwestern University, Evanston, Illinois 60208, USA*
[2]*State University of New York at Albany, Albany, New York 12222, USA*
[3]*University of Oklahoma, Norman, Oklahoma 73019, USA*
[4]*University of Pittsburgh, Pittsburgh, Pennsylvania 15260, USA*
[5]*University of Puerto Rico, Mayaguez, Puerto Rico 00681*
[6]*Purdue University, West Lafayette, Indiana 47907, USA*
[7]*Rensselaer Polytechnic Institute, Troy, New York 12180, USA*
[8]*University of Rochester, Rochester, New York 14627, USA*
[9]*Southern Methodist University, Dallas, Texas 75275, USA*
[10]*Syracuse University, Syracuse, New York 13244, USA*
[11]*Vanderbilt University, Nashville, Tennessee 37235, USA*
[12]*Wayne State University, Detroit, Michigan 48202, USA*
[13]*Carleton University, Ottawa, Ontario, Canada K1S 5B6*
[14]*Carnegie Mellon University, Pittsburgh, Pennsylvania 15213, USA*
[15]*Enrico Fermi Institute, University of Chicago, Chicago, Illinois 60637, USA*
[16]*Cornell University, Ithaca, New York 14853, USA*
[17]*University of Florida, Gainesville, Florida 32611, USA*
[18]*George Mason University, Fairfax, Virginia 22030, USA*
[19]*University of Illinois, Urbana-Champaign, Illinois 61801, USA*
[20]*Indiana University, Bloomington, Indiana 47405, USA*
[21]*University of Kansas, Lawrence, Kansas 66045, USA*
[22]*Luther College, Decorah, Iowa 52101, USA*
[23]*University of Minnesota, Minneapolis, Minnesota 55455, USA*
(Received 5 December 2007; published 20 June 2008)

Using a sample of 1.8 million $D\bar{D}$ mesons collected at the $\psi(3770)$ with the CLEO-c detector, we study the semileptonic decays $D^0 \to \pi^- e^+ \nu_e$, $D^+ \to \pi^0 e^+ \nu_e$, $D^0 \to K^- e^+ \nu_e$, and $D^+ \to \bar{K}^0 e^+ \nu_e$. For the total branching fractions we find $\mathcal{B}(D^0 \to \pi^- e^+ \nu_e) = 0.299(11)(9)\%$, $\mathcal{B}(D^+ \to \pi^0 e^+ \nu_e) = 0.373(22)(13)\%$, $\mathcal{B}(D^0 \to K^- e^+ \nu_e) = 3.56(3)(9)\%$, and $\mathcal{B}(D^+ \to \bar{K}^0 e^+ \nu_e) = 8.53(13)(23)\%$, where the first error is statistical and the second systematic. In addition, form factors are studied through fits to the partial branching fractions obtained in five q^2 ranges. By combining our results with recent unquenched lattice calculations, we obtain $|V_{cd}| = 0.217(9)(4)(23)$ and $|V_{cs}| = 1.015(10)(11)(106)$, where the final error is theoretical.

DOI: 10.1103/PhysRevD.77.112005 PACS numbers: 12.15.Hh, 13.20.Fc, 14.40.Lb

I. INTRODUCTION

In the standard model of particle physics, mixing of the quark mass eigenstates in their charged current interactions is described by the Cabibbo Kobayashi Maskawa (CKM) matrix [1]. This 3×3 quark mixing matrix must be unitary and can be described by four independent parameters. If the standard model is complete, experimental determination of the CKM matrix elements should verify its unitarity. Deviations from unitarity would indicate the presence of physics beyond the standard model. A variety of *CP*-conserving and *CP*-violating observables probe the elements of the CKM matrix and allow us to over-constrain it. Many of the key observables require great precision or great sensitivity to provide the constraints at the level needed to test the validity of the standard model description. It thus remains a continuing experimental challenge to test the unitarity of the CKM matrix fully.

Study of the semileptonic decay of D mesons plays a primary role in our understanding of the CKM matrix. These decays allow robust determination of the CKM matrix elements $|V_{cs}|$ and $|V_{cd}|$ by combining measured branching fractions with form factor calculations, such as those based on unquenched lattice QCD (LQCD) [2]. In addition, these measurements will provide precision tests of LQCD itself [3]. One approach to tests of LQCD assumes unitarity of the CKM matrix and compares the constrained matrix elements [4] to elements obtained with a combination of CLEO-c measurements and lattice form factors. A second approach, which is independent of CKM elements and thus free from the unitarity assumption, compares the measured and calculated ratios of semileptonic and purely leptonic branching fractions. Verification of lattice calculations at the few percent level will provide validation for use of the lattice in the B system, where they are relied upon for several crucial theoretical quantities.

This article presents a study of the $D^0 \to \pi^- e^+ \nu_e$, $D^+ \to \pi^0 e^+ \nu_e$, $D^0 \to K^- e^+ \nu_e$, and $D^+ \to \bar{K}^0 e^+ \nu_e$ decay modes (charge conjugate modes implied). A summary of the analysis is also provided in a shorter companion article [5]. The results are based on a sample of 1.8 million $D\bar{D}$ pairs collected with the CLEO-c detector at the Cornell Electron Storage Ring (CESR) from 281 pb^{-1} of e^+e^- data at the $\psi(3770)$ resonance. The sample is a superset of, and approximately 5 times larger than, the data used to obtain the first CLEO-c semileptonic branching-fraction measurements [6]. For each mode we determine the partial branching fractions in five q^2 ranges, with the sum of the five rates determining the total branching fraction. Fits to the rates determine the form factor shapes. By incorporating LQCD calculations into the form factor fits, we extract values for the CKM elements $|V_{cd}|$ and $|V_{cs}|$. Previous quenched lattice predictions carried errors of about 20%. Current unquenched LQCD calculations allow theoretical evaluation of the form factors at the 10% [2] level, with future improvement to the few percent level expected.

Within this article, Sec. II provides an overview of the formalism for exclusive semileptonic decays of charm mesons and their associated form factors. Sections III, IV, V, and VI cover the experimental procedures for event reconstruction and extraction of the branching fractions, the systematic uncertainty evaluation, and the branching-fraction results. Sections VII and VIII explore the form factor shape constraints from our data and the extraction of $|V_{cs}|$ and $|V_{cd}|$. Section IX presents our conclusions and comparisons with previous measurements.

II. EXCLUSIVE CHARMED SEMILEPTONIC DECAYS

The matrix element describing the semileptonic decay of a D meson to a pseudoscalar meson P is of the form

$$\mathcal{M}(D \to P e^+ \nu_e) = -i \frac{G_F}{\sqrt{2}} V_{cq}^* L^\mu H_\mu, \tag{1}$$

where G_F is the Fermi constant, V_{cq} is the appropriate CKM matrix element, and L^μ and H_μ are the leptonic and hadronic currents. The leptonic current can be written in terms of the electron and neutrino Dirac spinors, u_e and v_ν,

$$L^\mu = \bar{u}_e \gamma^\mu (1 - \gamma_5) v_\nu. \tag{2}$$

In the case of pseudoscalar decays, where there is no axial-vector contribution, the hadronic current is given by

$$H_\mu = \langle P(p) | \bar{q} \gamma_\mu c | D(p') \rangle, \tag{3}$$

where p' and p are the four-momenta of the parent D meson and the daughter P meson, respectively. The hadronic current is fundamentally a nonperturbative quantity that is difficult to evaluate. We can, however, reparametrize the current by expressing it in terms of the independent four-momenta in the process, which for a pseudoscalar-to-pseudoscalar decay are the two four-momenta $p' + p$ and $q = p' - p$. We can identify q as the four-momentum of the virtual W boson. A typical formulation of the hadronic current in terms of these four-momenta is given by

$$\langle P(p) | \bar{q} \gamma^\mu c | D(p') \rangle = f_+(q^2) \left[(p' + p)^\mu - \frac{M_D^2 - m_P^2}{q^2} q^\mu \right] + f_0(q^2) \frac{M_D^2 - m_P^2}{q^2} q^\mu, \tag{4}$$

where M_D is the mass of the D meson and m_P is the mass of the final state pseudoscalar meson. The nonperturbative contributions are incorporated in the scalar functions $f_+(q^2)$ and $f_0(q^2)$, the form factors of the decay. Kinematic constraints require $f_+(0) = f_0(0)$. A further simplification arises due to the small mass of the electron because $q^\mu L_\mu \to 0$ in the limit $m_e \to 0$. Thus including only the f_+ form factor in the hadronic current,

$$\langle P(p)|\bar{q}\gamma^{\mu}c|D(p')\rangle = f_+(q^2)(p'+p)^{\mu}, \quad (5)$$

is a very good approximation. With this form for the hadronic current the partial decay width becomes

$$\frac{d\Gamma(D \to Pe\nu_e)}{dq^2} = \frac{G_F^2|V_{cq}|^2}{24\pi^3}p^3|f_+(q^2)|^2. \quad (6)$$

The partial decay width [Eq. (6)] clearly reveals that extraction of the CKM matrix elements from measured rates requires prediction of the semileptonic form factors. Theoretical calculation of the form factors therefore has become a considerable industry. We focus here on parametrizations of the form factors that we employ in our form factor studies and in extraction of $|V_{cd}|$ and $|V_{cs}|$.

The goal of any particular parametrization of the semileptonic form factors is to provide an accurate, and physically meaningful, expression of the strong dynamics in the decays. To that end, one may express the form factors in terms of a dispersion relation, an approach that has been well established in the literature (see, for example, Ref. [7] and references therein). It is common to write the dispersive representation in terms of an explicit pole and a sum of effective poles

$$f_+(q^2) = \frac{f_+(0)}{1-\alpha}\frac{1}{1-\frac{q^2}{m_{\rm pole}^2}} + \sum_{k=1}^{N}\frac{\rho_k}{1-\frac{1}{\gamma_k}\frac{q^2}{m_{\rm pole}^2}}, \quad (7)$$

where ρ_k and γ_k are expansion parameters. Given the underlying $c \to q$ quark transition of the semileptonic decay, the mass $m_{\rm pole}$ is the mass of the lowest-lying $c\bar{q}$ vector meson. The parameter α gives the contribution from the vector-meson pole at $q^2 = 0$. Using this dispersion relation the true form factor can be approximated to any desired degree of accuracy by keeping sufficient terms in the expansion. This approach has the drawback that the decay dynamics are not explicitly predicted. Additionally, experimental data have suggested the need for only a few parameters in the description of the form factor shape. It is therefore natural to seek simplifications of this parametrization that can still capture the correct dynamics.

Removing the sum over effective poles entirely, leaving only the explicit vector-meson pole, provides one simplification route that is typically referred to as ''nearest pole dominance'' or ''vector-meson dominance.'' The resulting ''simple pole'' parametrization of the form factor is given by

$$f_+(q^2) = \frac{f_+(0)}{(1-\frac{q^2}{m_{\rm pole}^2})}. \quad (8)$$

Experimental data disagree with the physical basis for this approximation, since measurements of the parameter $m_{\rm pole}$ that fit the data do not agree with the expected vector-meson masses [8]. Effectively, at low or medium values of q^2 the spectrum is distorted compared to the simple pole model, receiving contributions from the continuum of effective poles above the lowest-lying pole mass.

The modified pole, or Becirevic-Kaidalov (BK) parametrization [9], was proposed to address this problem. The parametrization keeps the first term from the effective pole expansion, while making simplifications such that the form factor can be expressed using only two parameters: the intercept $f_+(0)$ and an additional shape parameter.[1] The parametrization is typically expressed in the form

$$f_+(q^2) = \frac{f_+(0)}{(1-\frac{q^2}{m_{\rm pole}^2})(1-\alpha\frac{q^2}{m_{\rm pole}^2})}. \quad (9)$$

This parametrization has recently been widely used in the extraction of semileptonic form factors from experimental measurements [10–13]. In addition, some recent LQCD calculations of the form factor have relied on this parametrization for extrapolation and interpolation purposes [2,14]. This scheme requires several assumptions to reduce the multiple parameters initially present [Eq. (7)] to one. The BK ansatz assumes that the gluon hard-scattering contributions (δ) are close to zero and that scaling violations (β) are close to unity, which may be succinctly expressed as

$$1 + 1/\beta - \delta \equiv \frac{(M_D^2 - m_P^2)}{f_+(0)}\frac{df_+}{dq^2}\bigg|_{q^2=0} \sim 2. \quad (10)$$

Once again, however, the experimental data do not bear out these assumptions [8]. We should observe $\alpha \sim 1.75$ in order to obtain $1 + 1/\beta - \delta = 2$, whereas the observed data are removed from such values by many standard deviations.

We note that both functional forms can provide adequate parametrizations of the data if their parameters are allowed to be nonphysical. Without a physical underpinning for the parametrization, however, parameters obtained from theory and/or from different experiments may not agree if their form factor sensitivities differ as a function of q^2.

Our primary form factor shape analysis therefore utilizes a series expansion around $q^2 = t_0$ that has been advocated by several groups for a physical description of heavy meson form factors [7,15–17]. The series expansion is congruous with the dispersion relations, and is guaranteed to contain the true form factor, yet is still rich enough to describe all variations that affect the physical observables.

To achieve a convergent series, the expansion is formulated as an analytic continuation of the form factor into the complex $t = q^2$ plane. There is a branch cut on the real axis for $t > (M_D + M_{K,\pi})^2$ that is mapped onto the unit circle by the variable z, defined as

[1]There will be three parameters if the $f_0(q^2)$ form factor, which we are neglecting due to the small electron mass, is also taken into account.

$$z(q^2, t_0) = \frac{\sqrt{t_+ - q^2} - \sqrt{t_+ - t_0}}{\sqrt{t_+ - q^2} + \sqrt{t_+ - t_0}}, \quad (11)$$

where $t_\pm \equiv (M_D \pm m_{K,\pi})^2$ and t_0 is the (arbitrary) q^2 value that maps to $z = 0$. The expression for the form factor becomes

$$f_+(q^2) = \frac{1}{P(q^2)\phi(q^2, t_0)} \sum_{k=0}^{\infty} a_k(t_0)[z(q^2, t_0)]^k, \quad (12)$$

with

$$P(q^2) \equiv \begin{cases} 1, & D \to \pi \\ z(q^2, M^2_{D_s^*}), & D \to K \end{cases}. \quad (13)$$

The $P(q^2)$ factor accommodates subthreshold resonances, which overcomes the convergence issues that a naive expansion would face with a nearby pole. Good convergence properties are expected since the physical region is restricted to $|z| < 1$. The physical observables do not depend on the choice of $\phi(q^2, t_0)$, which can be any analytic function, or on the value of t_0. We report a_k parameters that correspond to $t_0 = 0$ and the "standard" choice for ϕ (see, *e.g.* Ref. [17] and Appendix A), which results from bounding $\sum a_k^2$ from unitarity considerations. Appendix A presents results for an alternate choice of t_0 that minimizes the maximum value of $|z|$ over the physical range. If the series converges quickly, as expected, it is likely that only the first two or three terms will be able to be seen in the data. We will explore the number of terms needed to adequately describe our data.

While our primary form factor and CKM results will be based on the series expansion, we will also provide results based on the two pole parametrizations for comparative purposes.

III. EVENT RECONSTRUCTION AND SELECTION

The analysis technique rests upon association of the missing energy and momentum in an event with the neutrino four-momentum [18], an approach enabled by the excellent hermeticity and resolution of the CLEO-c detector [3,19]. Charged particles are detected over 93% of the solid angle by two wire tracking chambers within a 1.0 T solenoid magnet. The momentum resolution is 0.6% at 800 MeV/c. Specific ionization measurements from the tracking system in combination with a ring imaging Čerenkov detector (RICH) [20] provide particle identification. A CsI(Tl) crystal electromagnetic calorimeter provides coverage over about 93% of 4π, and achieves a typical π^0 mass resolution of 6 MeV/c^2.

Electron candidates are identified above 200 MeV/c over 90% of the solid angle by combining information from specific ionization with calorimetric, RICH, and tracking measurements. The identification efficiency, which has been determined from data, is greater than 96% above 500 MeV/c and greater than 90% above 300 MeV/c. The average probability that a hadron is misidentified as an electron is less than 0.8%. Below 300 MeV/c the efficiency falls rapidly, reaching 60% in the 200–250 MeV/c region. To reduce our sensitivity to final state radiation (FSR), we add photons within 3.5° of the initial electron momentum back into the tracking-based four-momentum.

Charged pions and kaons from the signal decay are identified using specific ionization and RICH measurements. Pion candidates below 750 MeV/c and kaon candidates below 500 MeV/c are identified using only specific ionization information, which is required to be within 3 standard deviations (σ) of that expected for the assigned particle type. For pion candidates above 650 MeV/c, we also require the pion mass hypothesis to be more likely than the kaon mass hypothesis. Above these momenta, candidate tracks must also pass RICH identification criteria. Specifically, we require that pion (kaon) candidates are more than 3σ closer to a pion (kaon) hypothesis than a kaon (pion) hypothesis.

A π^0 candidate must have a $\gamma\gamma$ mass within 2.5σ of the π^0 mass. K^0_S candidates are reconstructed using a constrained vertex fit to candidate $\pi^+\pi^-$ daughter tracks. The $\pi^+\pi^-$ mass must be within 4.5σ of the K^0_S mass.

To reconstruct the undetected neutrino we utilize the hermeticity of the CLEO-c detector to find the missing energy and momentum. In the process $e^+e^- \to \psi(3770) \to D\bar{D}$, the total energy of the beams is imparted to the $D\bar{D}$ system. Because the beam energies are symmetric and the beam crossing angle is small at CESR, each produced D has an energy equal, on average, to the beam energy.[2] The missing four-momentum in an event is given by $p_{\rm miss} = (E_{\rm miss}, \vec{p}_{\rm miss}) = p_{\rm total} - \sum p_{\rm charged} - \sum p_{\rm neutral}$, where the event four-momentum $p_{\rm total}$ is known from the energy and crossing angle of the CESR beams. Charged and neutral particles for the sums must pass selection criteria designed to achieve the best possible $|\vec{p}_{\rm miss}|$ resolution by balancing the efficiency for detecting true particles against the rejection of false ones.

For the charged four-momentum sum, $\sum p_{\rm charged}$, optimal selection is achieved with topological criteria. These criteria minimize multiple counting that can result from low-momentum tracks that curl in the magnetic field, charged particles that decay in flight or interact within the detector, and spurious tracks. Tracks that are actually segments of a single low transverse momentum "curling" particle are identified by selecting reconstructed track pairs with opposite curvature whose innermost and outermost diametric radii each match within 14 cm and whose separation in ϕ is within 180° ± 20°. For physics use we select the track segment that will best represent the original charged particle based on track quality and distance-of-closest-approach to the beam spot. We employ similar

[2]A small correction to account for the crossing angle is necessary.

algorithms to identify particles that curl more than once, creating three or more track segments. We also identify tracks that have scattered or decayed in the drift chamber, causing the original track to end and one or more tracks to begin in a new direction. We keep only the track segment with the majority of its hits before the interaction point. Spurious tracks are identified by their low hit density and/or low number of overall hits and rejected.

Each hadronic track must be assigned a mass hypothesis to calculate its contribution to the total energy sum. We assign a most probable mass hypothesis by combining detector measurement with particle production information. The production information is introduced because at a momentum where many more pions than kaons are produced, it is statistically advantageous to identify a track as a kaon only when the detector's particle identification information strongly favors a kaon. For each track, we first calculate a likelihood for the kaon and pion hypothesis based on specific ionization and RICH measurements. Those likelihoods are then weighted by the Monte Carlo (MC) prediction for the relative K^- and π^- abundances in D decays at that track's momentum, which then gives us the true probability for each mass hypothesis.

For the neutral four-momentum sum, $\sum p_{\rm neutral}$, clusters resulting from the interactions of charged hadrons must be avoided. As a first step, calorimeter showers passing the standard CLEO proximity matching (within 15 cm of a charged track) are eliminated. Optimizations also revealed that all showers under 50 MeV should be eliminated. The processes that result in reconstructed showers (''split-offs'') separate from but within about 25° of a proximity-matched shower tend to result in an energy distribution over the 3×3 central array of the split-off shower that ''points back'' to the core hadronic shower. We combine this information with the ratio of energies in the 3×3 to 5×5 arrays of crystals, whether the shower forms a good π^0, and the MC predictions for relative spectra for true photons versus split-off showers to provide an optimal suppression of the contribution.

Association of the missing four-momentum with the neutrino four-momentum is only accurate if the event contains no more than one neutrino and if all true particles are detected. For events with additional missing particles or doubly-counted particles, the signal modes tend not to reconstruct properly while background processes tend to smear into our sensitive regions. Hence, it is worthwhile to reject events for which independent measures indicate these problems. We therefore exclude events that have either more than one electron[3] or nonzero net charge. Multiple electrons indicate an increased likelihood for multiple neutrinos, while a nonzero net charge indicates at least one missed or doubly-counted charged particle.

[3]Muons from semimuonic decay range out before reaching the CLEO muon detectors.

After application of the above criteria approximately 90% of the signal MC $|\vec{p}_{\rm miss}|$ distribution is contained in a central core with $\sigma \sim 15$ MeV/c.

To further enhance the association of the missing momentum with an undetected neutrino in our final event sample, we require that the $M^2_{\rm miss} \equiv E^2_{\rm miss} - |\vec{p}_{\rm miss}|^2$ be consistent with a massless neutrino. The $M^2_{\rm miss}$ resolution,

$$\sigma(M^2_{\rm miss}) = 2E_{\rm miss}\sigma(E_{\rm miss}) \oplus 2|\vec{p}_{\rm miss}|\sigma(|\vec{p}_{\rm miss}|),$$

is dominated by the $E_{\rm miss}$ term since the resolution of $|\vec{p}_{\rm miss}|$ is roughly half that of $E_{\rm miss}$. MC simulation indicated an optimal requirement of $|M^2_{\rm miss}/2|\vec{p}_{\rm miss}|| < 0.2$ GeV/c^3, which (noting $E_{\rm miss} \approx |\vec{p}_{\rm miss}|$ for signal) provides selection at approximately constant $E_{\rm miss}$ resolution. Additionally, because of the superior $|\vec{p}_{\rm miss}|$ resolution, in subsequent calculations we take $p_\nu \equiv (|\vec{p}_{\rm miss}|, \vec{p}_{\rm miss})$.

Semileptonic decays $D \to Pe\nu$, where P is a pion or kaon, are identified by their consistency with the expected D energy and momentum. Candidates are selected based on $\Delta E \equiv (E_P + E_e + E_\nu) - E_{\rm beam}$ (expected to be zero within our resolution of about 20 MeV) and yields are extracted from the resulting distributions in beam-constrained mass $M_{\rm bc}$ (equivalent to D momentum and expected to be close to the known D mass). These quantities are corrected for the small boost resulting from the 3 mrad beam crossing angle. Because the $|\vec{p}_\nu|$ resolution dominates the ΔE resolution, the factor ζ satisfying $(E_P + E_e + \zeta E_\nu) - E_{\rm beam} = 0$ provides a scalar improvement to $\vec{p}_\nu = \vec{p}_{\rm miss}$. We therefore substitute $\zeta\vec{p}_\nu$ for $\vec{p}_\nu$ in the beam-constrained mass calculation: $M_{\rm bc} \equiv \sqrt{E^2_{\rm beam} - |\vec{p}_P + \vec{p}_e + \zeta\vec{p}_\nu|^2}$. The resulting resolution for $M_{\rm bc}$ is 4 MeV/c^2.

Selection criteria were optimized by studying MC samples independent of those used elsewhere in the analysis. Sources of backgrounds include events with fake electrons, noncharm continuum production ($e^+e^- \to q\bar{q}$, $e^+e^- \to \tau^+\tau^-$, and $e^+e^- \to \gamma\psi(2S)$), and $D\bar{D}$ processes other than signal.

The optimal ΔE requirement was determined to be $-0.06 < \Delta E < 0.10$ GeV. For the Cabibbo-favored modes, the background level remaining after this selection is only a few percent of the signal level. For the Cabibbo-suppressed modes, there remains significant background from cross feed among the signal modes, particularly from the kaon modes, as well as from the related modes $D^+ \to K^0_L e^+\nu_e$ and $D^+ \to K^0_S e^+\nu_e$ where $K^0_S \not\to \pi^+\pi^-$. Since the cross feed typically involves particles from the ''other D'' decay, we obtain some suppression of this background with a q^2-dependent requirement on $\Delta E_{\rm n.s.}$ for the non-signal particles in the event. We obtain $\Delta E_{\rm n.s.}$ by summing the energy of all nonsignal particles in an event, even though we do not specifically reconstruct the nonsignal D decay. This criterion effectively imposes an additional constraint on the quality of the reconstructed neutrino.

TABLE I. The fraction of candidates affected by the multiple candidate restrictions, either because a different mode satisfied the criteria (''other mode loss''), or because there was a better candidate in the same mode (''same mode loss'').

Mode	Other mode loss (%)	Same mode loss (%)
$\pi^- e^+ \nu_e$	5.5	3.8
$K^- e^+ \nu_e$	2.2	0.7
$\pi^0 e^+ \nu_e$	6.7	6.2
$K^0_S e^+ \nu_e$	0.8	7.2

To further suppress cross feed backgrounds, particularly from the Cabibbo-favored into the Cabibbo-suppressed modes, as well as to simplify the statistical interpretation of our results, we allow only one D^0 candidate with $M_{\rm bc} > 1.794$ GeV$/c^2$ in an event, and/or only one D^+ candidate with $M_{\rm bc} > 1.794$ GeV$/c^2$ in an event. This restriction only affects the final state hadron; there is a unique $\ell\nu$ pair in a candidate event. For events with multiple D^+ candidates or multiple D^0 candidates, we choose the candidate with the smallest $|\Delta E|$, independent of q^2. We also require a $D^+ \to \pi^0 e^+ \nu_e$ candidate to have the smallest $|\Delta E|$ compared to any other final state candidates in the event, and that these events contain no reconstructed $D^0 \to K^- e^+ \nu_e$ candidate. These additional criteria suppress cross feed from the charged pion and kaon modes with almost no loss of true $\pi^0 e^+ \nu_e$ decays. Table I summarizes the fraction of candidates affected in each mode as a result of these requirements. The average background level (q^2-dependent) in the pion modes is about 20% of the signal level.

From the measured electron and the rescaled neutrino four-momenta we calculate $q^2 \equiv M^2_{W^*}$ from $q^2 = (p_\nu + p_e)^2$. The resulting resolution is 0.01 GeV$^2/c^4$, independent of q^2.

IV. EXTRACTION OF BRANCHING FRACTIONS

A. Method and Binning

For each of the four signal modes we construct the $M_{\rm bc}$ distributions in five q^2 ranges: $q^2 < 0.4$ GeV$^2/c^4$, $0.4 \le q^2 < 0.8$ GeV$^2/c^4$, $0.8 \le q^2 < 1.2$ GeV$^2/c^4$, $1.2 \le q^2 < 1.6$ GeV$^2/c^4$, and $q^2 \ge 1.6$ GeV$^2/c^4$. These 20 distributions are fit simultaneously to extract the partial branching fraction for each interval. The total branching fraction is then obtained in each mode by summing its five partial branching fractions. Fitting in five q^2 ranges minimizes the experimental sensitivity of the total branching fractions to form factor shape uncertainties, while simultaneous fitting of all four modes ensures self-consistent handling of the cross feed backgrounds among the modes.

The fit utilizes a binned maximum likelihood approach extended to include the finite statistics of the MC samples following the method of Barlow and Beeston [21]. The $M_{\rm bc}$ distribution is divided into 14 uniform bins over the range $1.794 < M_{\rm bc} < 1.878$ GeV$/c^2$.

B. Fit Components and Parameters

We fit the data to the signal components and five background components. The signal mode components are obtained from MC generated using EvtGen [22] and modified pole-model form factors [9] with parameters from the most recent LQCD results [2]. We apply several corrections to our GEANT-based [23] MC samples to improve simulation of the neutrino-reconstruction procedure.

From independent studies, mostly based on CLEO-c samples with one fully reconstructed hadronic D decay, we evaluate corrections and associated systematic uncertainties for simulation of hadronic showers, false charged particles, and charged-particle identification. We find that the simulations of charged particles, charged-particle momentum resolution, and photon-energy resolution need no correction, though we include the uncertainties in the systematic uncertainty evaluation. We reweight the MC samples to correct the rate and spectrum for K^0_L production (which affects the neutrino-reconstruction efficiency), for π^0 and π^- production in our full D decay model, and for the momentum-dependent rate at which a K^- fakes a π^-. All of these corrections affect the cross feed background rates into and between the Cabibbo-suppressed modes. They lead to few percent (or less) changes in the measured yields, but are determined to better than 10% of themselves.

In the MC samples we select only true electrons (reconstructed tracks that have been matched to a generator-level electron) with a probability for acceptance given by data-measured efficiencies described earlier. We thereby exclude from the MC any events caused by identification of a fake electron and instead estimate this background using data, as we describe in detail below. This procedure eliminates any reliance on MC predictions for either electron efficiency or the rate at which hadrons fake electrons.

We are sensitive to the distortion of efficiency and kinematics in our signal modes due to FSR. Our signal MC sample therefore includes FSR distributed according to the kaon leading-order radiation (KLOR) [24] calculation applied to charm decay.

For each reconstructed q^2 interval in a given mode, we generate a MC sample in the same (generator level) q^2 interval, to which the full analysis is applied. That is, we obtain the full set of 20 reconstructed $M_{\rm bc}$ distributions from each of these 20 independent samples. For each of the generated q^2 intervals, a single floating parameter, which corresponds to the efficiency-corrected data yield in that interval, controls the normalization of all its 20 reconstructed distributions. The relative normalizations among those reconstructed distributions remains fixed at the level predicted by our corrected MC simulation. Because the signal rate in each reconstructed range drives the normalization for the corresponding generated q^2 interval, the data in effect fix the cross feed rates into the other 19 reconstructed distributions.

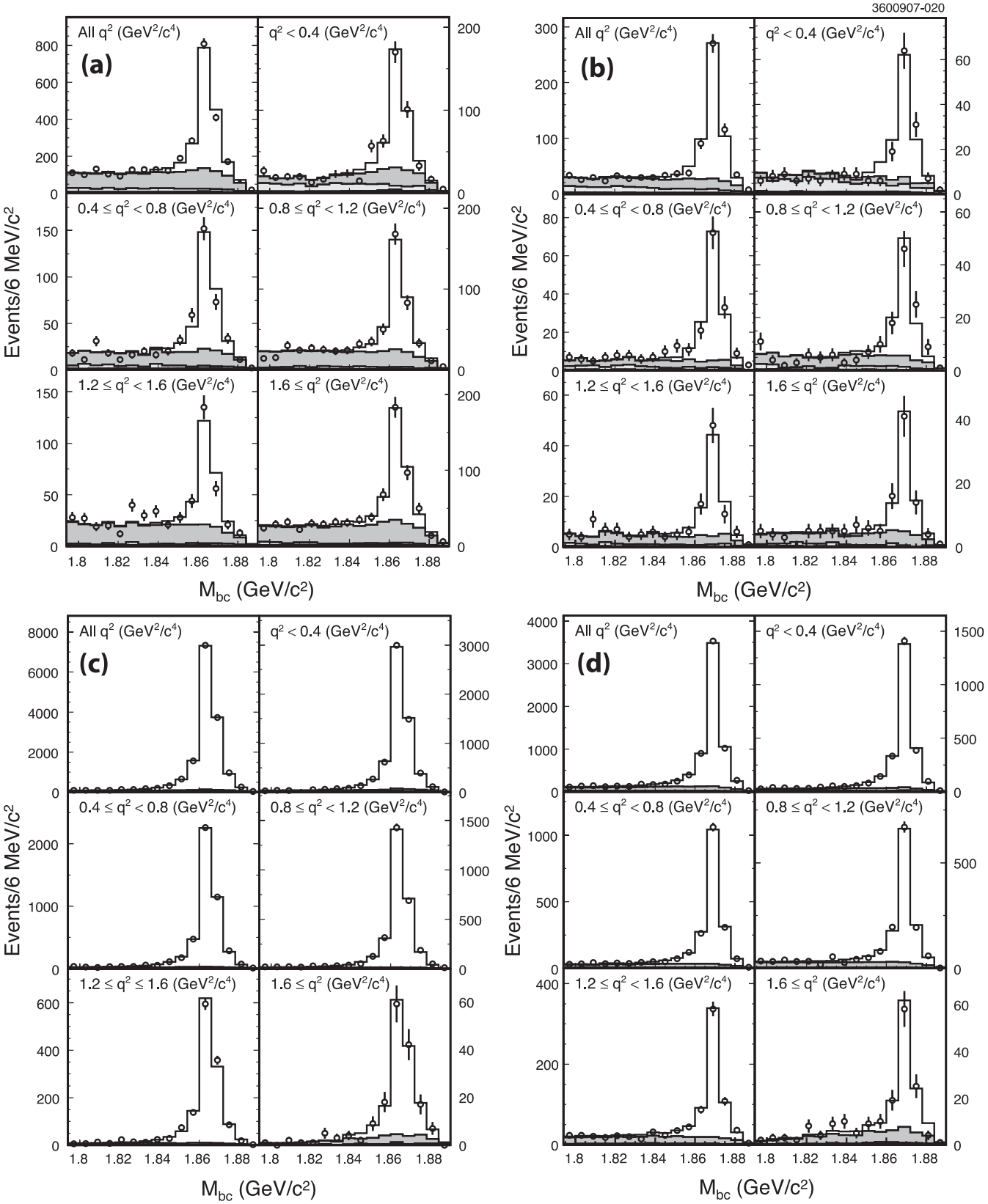

FIG. 1. $M_{\rm bc}$ distributions for the modes (a) $D^0 \to \pi^- e^+ \nu_e$, (b) $D^+ \to \pi^0 e^+ \nu_e$, (c) $D^0 \to K^- e^+ \nu_e$, and (d) $D^+ \to K^0_S e^+ \nu_e$. The data are shown by the points, and the fit components (histograms) are normalized using the nominal fit results (see text): signal MC (clear), cross feed and nonsignal $D\bar{D}$ MC (gray), continuum MC (light gray), and fake e^+ (black).

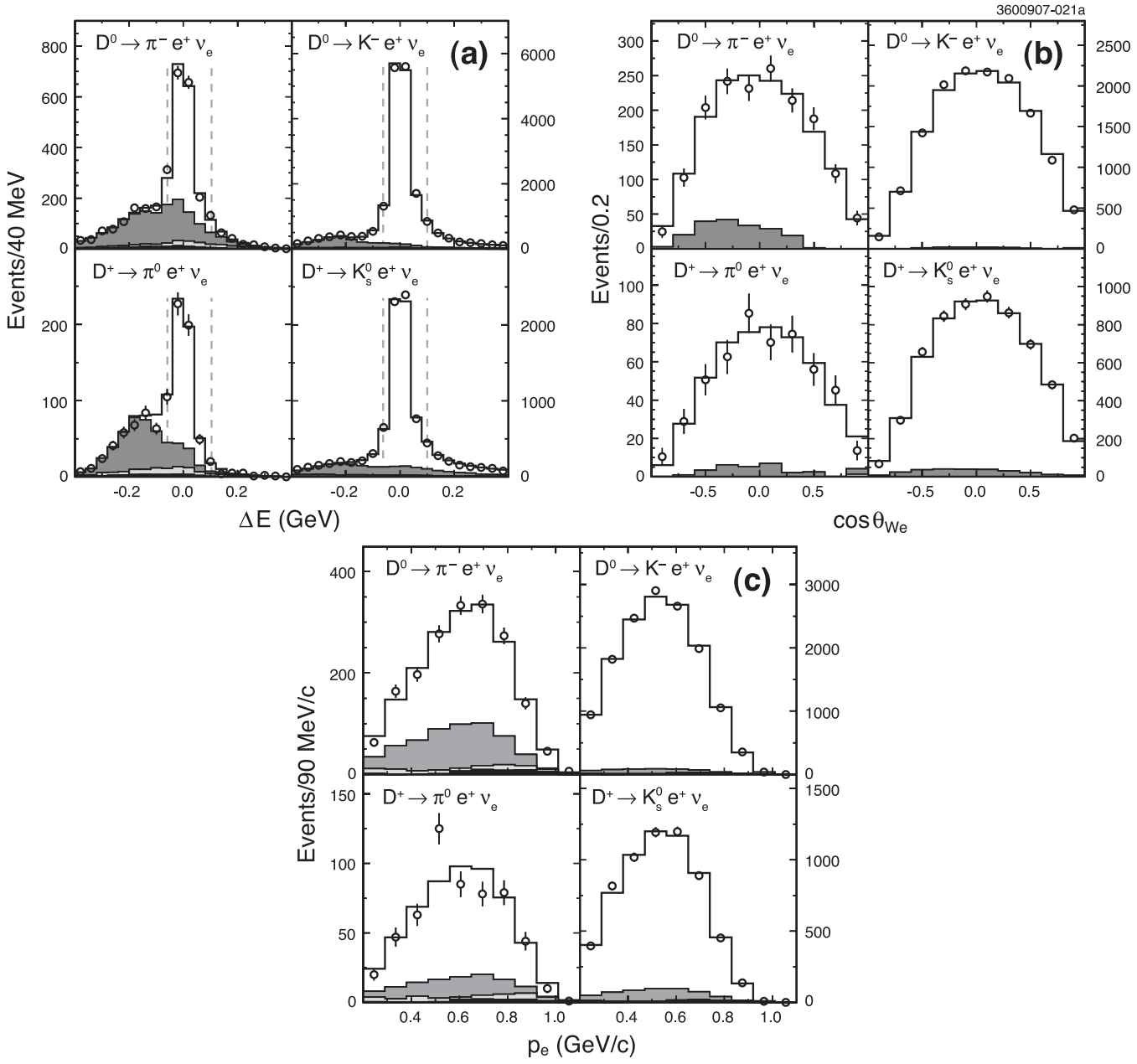

FIG. 2. The kinematic distributions for (a) ΔE, (b) $\cos\theta_{We}$, and (c) p_e, for events falling within the $M_{\rm bc}$ signal region for each of the four signal modes. The data are shown by the points, and the fit components (histograms) are normalized using the nominal fit results (see text): signal MC (clear), cross feed and nonsignal $D\bar{D}$ MC (gray), continuum MC (light gray), and fake e^+ (black). The dotted lines in (a) indicate for each mode the ΔE region used in fitting.

We also use MC samples to describe the $D\bar{D}$ background and the three continuum contributions. We normalize the continuum components according to their cross sections at the $\psi(3770)$ and the measured data luminosity. The nonsignal $D\bar{D}$ sample was generated using EvtGen, with decay parameters updated to reflect our best knowledge of D meson decays. This component floats separately for each reconstructed final state, but the relative rates over the five q^2 regions within that state are fixed. This approach helps to reduce our sensitivity to inaccuracies in the D decay model. Finally, we input MC components for $D^+ \to K^0_L e^+ \nu_e$ and $D^+ \to K^0_S(\pi^0\pi^0)e^+\nu_e$. The normalization of each of these components in a given q^2 interval is tied to the fit parameter for the $D^+ \to K^0_S(\pi^+\pi^-)e^+\nu_e$ mode in that q^2 interval via known amplitude or branching-fraction ratios.

The contributions from events in which hadrons have faked the signal electron are evaluated using data. The momentum-dependent electron identification fake rates from pions and kaons are measured using a variety of

TABLE II. Results of fit to $D\bar{D}$ MC sample with statistics equivalent to 40 times the data luminosity. $Y_{\rm input}$ is the true yield, $Y_{\rm fit}$ the efficiency-corrected yield from the fit, and $\sigma_{Y_{\rm fit}}$ the 1σ error on the efficiency-corrected fit yield.

	$(Y_{\rm input} - Y_{\rm fit})\sigma_{Y_{\rm fit}}$ True q^2 interval (GeV$^2/c^4$)					
Decay	<0.4	0.4–0.8	0.8–1.2	1.2–1.6	≥ 1.6	All q^2
$\pi^- e^+ \nu_e$	0.55	−0.92	0.98	−0.33	1.16	0.51
$\pi^0 e^+ \nu_e$	−1.57	0.37	−0.55	0.85	0.98	−0.95
$K^- e^+ \nu_e$	−2.34	1.27	1.54	0.18	0.99	−0.14
$K^0_S e^+ \nu_e$	−0.29	−0.49	1.77	1.14	0.54	0.76

data samples. We obtain our background estimates by analyzing the subset of events in which we identify no electrons according to the criteria we apply in the multiple-lepton veto. For each track in turn in each of these events, we treat that track as the signal electron and fully analyze the event as described above. The contribution in each mode is then weighted according to the fake rate. The fake electron component is then added to the fit with a fixed, absolute, normalization.

Finally, we allow the fit to adjust the $M_{\rm bc}$ resolution in the $D^0 \to \pi^- e^+ \nu_e$, $D^+ \to \pi^0 e^+ \nu_e$, and $D^0 \to K^- e^+ \nu_e$ modes by applying a Gaussian smear to these distributions. As a result the signal MC $M_{\rm bc}$ resolution in these modes is increased from $\sim$3.5 MeV/c^2 to match the data resolution of $\sim$4 MeV/c^2. The $M_{\rm bc}$ resolution in the $D^+ \to K^0_S e^+ \nu_e$ signal MC matches the data resolution very well so we apply no additional smearing to this mode in the fit.

In summary we have 27 free parameters in the fit: the 20 signal rates, the four nonsignal $D\bar{D}$ normalizations, and the three $M_{\rm bc}$ smearing parameters. This leaves us with a total of $280 - 27 = 253$ degrees of freedom for the fit.

C. Checks and Results

The results for the fit to the $M_{\rm bc}$ distributions are displayed in Fig. 1. Our $-2\ln\mathcal{L}$ behavior should be approximately χ^2-like, and we find $-2\ln\mathcal{L} = 275.5$ for 253 degrees of freedom. Note that each of the 20 distributions is described by mainly one free parameter—the signal rate within that bin, with a more constrained contribution from the parameters (resolution and $D\bar{D}$ background rate) that float independently for each signal mode, with the relative contribution into each q^2 interval fixed within a mode. All other contributions are either explicitly or effectively fixed by other constraints.

Other important reconstructed kinematic variables are presented integrated over q^2 with the components scaled according to the nominal fit. Figure 2(a) shows the ΔE distributions for events within the signal-enhanced region $|M_{\rm bc} - M_D| < 0.015$ GeV/c^2. Figure 2(b) shows $\cos\theta_{We}$, the cosine of the angle between the W in the D rest frame and the electron in the W rest frame, in the signal $M_{\rm bc}$ and ΔE regions. All of our signal modes should exhibit a $\sin^2\theta_{We}$ dependence independent of the form factor though acceptance effects distort the reconstructed distribution. The fits describe the observed distributions very well. Finally we find that our fit generally agrees well with the observed momentum (p_e) spectrum for the signal electron (Fig. 2(c)). The poorest agreement is exhibited by the $\pi^0 e \nu_e$ mode, where the probability of χ^2 is still over 3%.

To test the fitting procedure, we fit a set of mock data with known input branching fractions created from the large $D\bar{D}$ MC sample (equivalent to $\sim$40 times the data luminosity) used to obtain our nonsignal $D\bar{D}$ background estimate. We fit the sample using distributions from our standard signal MC and from the nonsignal portion of the generic $D\bar{D}$ sample. Because our "data" in this case derives from the same underlying decay model and detector simulation as our fit inputs, we do not apply the corrections noted in the previous section that remove differences between data and our MC simulation.

Table II presents the differences between our measured and the generator-level rates. We see no biases at this greater level of sensitivity, demonstrating the reliability of the fitting procedure. Furthermore, the semileptonic modes in the generic MC sample used to simulate the "data" were generated using ISGW2 [25] form factors, which have a significantly different q^2 behavior than the LQCD-derived form factors [2] of our signal MC sample. Our test therefore also verifies that we have adequately subdivided the q^2 range to avoid significant dependence on input form factor modeling, even at levels significantly more sensitive than we can probe with the current data.

V. EXPERIMENTAL SYSTEMATIC UNCERTAINTIES

The systematic uncertainties for the D^0 modes are summarized in Tables III and IV. The first table presents the complete list, while the second breaks down the neutrino-reconstruction simulation errors into component parts. The corresponding systematics tables for the D^+ modes are presented in Tables V and VI. For individual uncertainties we give the sign of the error relative to the change in the lowest q^2 range. The largest systematic uncertainties are those associated with the number of $D\bar{D}$ pairs (needed for normalization in the branching-fraction determination, as described in Sec. VI) and with neutrino-reconstruction

TABLE III. Summary of full and partial branching-fraction systematic errors (%) for the $D^0 \to \pi^- e^+ \nu_e$ and $D^0 \to K^- e^+ \nu_e$ signal decay modes. The sign represents the direction of change relative to the change in the $[0, 0.4)$ GeV$^2/c^4$ interval in each mode.

	$D^0 \to \pi^- e^+ \nu_e \alpha$ q^2 interval (GeV$^2/c^4$)							$D^0 \to K^- e^+ \nu_e$ q^2 interval (GeV$^2/c^4$)						
Systematic	$[0, 0.4)$	$[0.4, 0.8)$	$[0.8, 1.2)$	$[1.2, 1.6)$	$[1.6, q^2_{\rm max}]$	All q^2		$[0, 0.4)$	$[0.4, 0.8)$	$[0.8, 1.2)$	$[1.2, 1.6)$	$[1.6, q^2_{\rm max}]$	All q^2	
Number $D\bar{D}$	1.51	1.51	1.51	1.51	1.51	1.51	1.51	1.51	1.51	1.51	1.51	1.51	1.51	
ν_e simulation	1.45	1.77	2.21	2.87	1.59	1.69	1.52	1.99	1.96	2.39	1.28	1.80		
π^0 efficiency	0.01	0.01	0.01	0.00	−0.03	−0.00	0.00	0.00	0.00	0.00	0.01	0.00		
K^0_S efficiency	0.01	−0.01	−0.02	−0.04	−0.08	−0.03	0.01	0.00	0.00	0.00	0.07	0.01		
π^- PID	0.44	0.41	0.39	0.39	0.40	0.41	0.00	0.00	0.00	0.00	0.00	0.00		
K^- PID	0.05	0.02	0.02	0.01	0.02	0.03	0.32	0.30	0.28	0.26	0.26	0.30		
e^+ PID	0.76	0.40	0.75	0.36	0.44	0.56	0.65	0.58	0.60	0.52	0.46	0.61		
e^+ Fakes	2.50	0.45	−0.01	0.05	0.92	0.88	0.57	0.07	−0.04	0.01	0.39	0.25		
π^0 production	0.01	0.02	0.03	0.01	0.06	0.03	0.00	0.00	−0.01	0.00	0.01	0.00		
π^- production	0.07	0.42	0.44	0.10	−1.96	−0.24	0.00	0.00	0.00	0.05	0.23	0.01		
K^- fakes	0.67	1.01	0.93	0.35	−0.08	0.58	0.00	0.00	−0.01	−0.01	−0.02	0.00		
$\pi^- e^+ \nu_e$ $M_{\rm bc}$ res.	0.93	1.06	0.85	0.83	1.05	0.95	0.02	0.01	0.01	0.01	0.06	0.01		
$K^- e^+ \nu_e$ $M_{\rm bc}$ res.	0.07	0.04	0.02	0.01	0.01	0.03	0.09	0.08	0.07	0.09	0.16	0.09		
$\pi^0 e^+ \nu_e$ $M_{\rm bc}$ res.	0.01	0.02	0.00	0.01	−0.13	−0.02	0.00	0.00	0.00	0.00	0.00	0.00		
e^+ veto	0.05	0.04	−0.01	−0.14	−0.01	0.00	0.08	0.07	0.00	−0.02	−0.03	0.05		
FSR	0.85	1.53	0.97	0.91	0.75	0.99	0.63	0.61	0.56	0.48	0.47	0.59		
Model dep.	0.50	−0.01	−0.09	0.43	−1.55	−0.19	0.33	−0.11	−0.16	−0.41	−1.29	0.02		
Total	3.70	3.26	3.26	3.56	3.74	2.95	2.44	2.66	2.63	2.95	2.51	2.53		

simulation. Uncertainties in neutrino simulation include both inaccuracies in detector simulation and uncertainty in the decay model of the nonsignal D, as discussed above.

The starting point for the assessment of many of the systematic uncertainties is the measurement of any discrepancies between data and MC in the desired quantities (e.g., signal pion efficiency, signal kaon efficiency, etc.). Such measurements (or limits) are made using an independent data sample—in most cases, a sample of events with one of the two D mesons from the $\psi(3770)$ fully reconstructed in a hadronic mode. In the case of significant discrepancies, the MC samples are corrected for use in our nominal fit (the fit used to obtain our final branching-fraction results, as opposed to any of the fits used to obtain systematic uncertainties) as noted above. Such corrections lead to changes in the measured yields of up to a few percent, but are determined precisely enough to yield subpercent systematic uncertainties. For each systematic category, we determine the size of its contribution by biasing the MC samples away from their nominal configuration at the level given by the uncertainty of the independent study. We refit the data with these biased MC samples, and use the deviation of the fit results from their nominal values to provide an estimate of the uncertainty. We note that because of the correlations among the five q^2 intervals in a given mode, the sum over q^2 of the systematic errors tends to be less sensitive to the systematic variations than the individual intervals themselves.

The number of $D\bar{D}$ pairs, used to convert the measured yields to branching fractions (see below), is a direct prod-

TABLE IV. Summary of full and partial branching-fraction systematic errors (%) associated with neutrino modeling in the MC for the $D^0 \to \pi^- e^+ \nu_e$ and $D^0 \to K^- e^+ \nu_e$ signal decay modes. The sign represents the direction of change relative to the change in the $[0, 0.4)$ GeV$^2/c^4$ interval in each mode.

	$D^0 \to \pi^- e^+ \nu_e$ q^2 interval (GeV$^2/c^4$)							$D^0 \to K^- e^+ \nu_e$ q^2 interval (GeV$^2/c^4$)						
ν Systematic	$[0, 0.4)$	$[0.4, 0.8)$	$[0.8, 1.2)$	$[1.2, 1.6)$	$[1.6, q^2_{\rm max}]$	All q^2		$[0, 0.4)$	$[0.4, 0.8)$	$[0.8, 1.2)$	$[1.2, 1.6)$	$[1.6, q^2_{\rm max}]$	All q^2	
Split-off showers	0.58	0.90	1.92	2.58	0.48	1.17	0.89	1.54	1.49	2.00	0.67	1.29		
K^0_L showers	0.15	0.13	0.11	0.06	−0.60	−0.04	0.01	−0.02	−0.04	−0.05	−0.06	−0.01		
K^0_L production	0.67	0.66	0.66	0.67	0.65	0.66	0.66	0.65	0.66	0.67	0.69	0.66		
Track efficiency	0.60	0.56	0.50	0.63	0.45	0.54	0.37	0.39	0.44	0.44	0.21	0.39		
Track resolution	0.00	1.02	0.01	0.46	0.85	0.46	0.28	0.43	0.50	0.60	0.34	0.39		
Split-off rejection	0.58	−0.02	0.16	0.04	−0.22	0.12	0.59	0.56	0.48	0.43	0.21	0.54		
Particle ID	0.01	−0.02	0.08	0.02	0.09	0.04	0.06	0.04	0.05	0.03	0.04	0.05		
Shower resolution	0.03	0.09	0.06	−0.01	0.11	0.06	0.00	0.00	0.00	0.00	−0.01	0.00		
Fake tracks	0.76	0.71	0.70	0.71	0.72	0.72	0.72	0.72	0.71	0.71	0.71	0.72		
Total	1.45	1.77	2.21	2.87	1.59	1.69	1.52	1.99	1.96	2.39	1.28	1.80		

TABLE V. Summary of full and partial branching-fraction systematic errors (%) for the $D^+ \to \pi^0 e^+ \nu_e$ and $D^+ \to \bar{K}^0 e^+ \nu_e$ signal decay modes. The sign represents the direction of change relative to the change in the $[0, 0.4)$ GeV$^2/c^4$ interval in each mode.

	$D^+ \to \pi^0 e^+ \nu_e$ q^2 interval (GeV$^2/c^4$)							$D^+ \to \bar{K}^0 e^+ \nu_e$ q^2 interval (GeV$^2/c^4$)						
Systematic	$[0, 0.4)$	$[0.4, 0.8)$	$[0.8, 1.2)$	$[1.2, 1.6)$	$[1.6, q^2_{\rm max}]$	All q^2		$[0, 0.4)$	$[0.4, 0.8)$	$[0.8, 1.2)$	$[1.2, 1.6)$	$[1.6, q^2_{\rm max}]$	All q^2	
Number $D\bar{D}$	1.60	1.60	1.60	1.60	1.60	1.60	1.60	1.60	1.60	1.60	1.60	1.60	1.60	1.60
ν simulation	2.54	3.41	2.57	2.53	2.45	1.96	1.71	1.75	1.82	1.84	2.18	1.74		
π^0 efficiency	0.87	0.56	0.77	1.07	1.07	0.85	0.00	0.01	−0.01	−0.02	0.00	0.00		
K^0_S efficiency	0.02	0.02	0.08	0.11	0.18	0.07	1.05	1.00	0.94	0.88	0.81	1.00		
π^- PID	0.17	0.37	0.13	−0.24	−0.29	0.06	0.01	0.01	0.00	−0.03	−0.02	0.00		
K^- PID	0.17	0.37	0.12	−0.24	−0.29	0.06	0.01	0.01	0.00	−0.02	0.00	0.00		
e^+ PID	1.13	0.56	0.33	0.98	0.01	0.62	0.62	0.65	0.52	0.59	0.76	0.61		
e^+ Fakes	1.52	0.14	−0.29	−0.07	0.64	0.44	0.38	−0.03	−0.17	0.09	1.00	0.14		
π^0 production	0.43	0.81	0.76	−0.73	−1.87	−0.04	0.02	−0.01	0.00	−0.11	−0.14	−0.01		
π^- production	0.07	−0.02	0.03	0.02	1.46	0.29	0.02	−0.01	0.00	0.19	1.12	0.04		
K^- fakes	0.01	−0.01	0.04	0.07	0.20	0.05	0.01	0.01	−0.03	−0.07	−0.16	−0.01		
$\pi^- e^+ \nu_e$ $M_{\rm bc}$ res.	0.00	0.00	−0.01	0.05	−0.29	−0.05	0.01	0.01	0.00	0.04	0.09	0.01		
$K^- e^+ \nu_e$ $M_{\rm bc}$ res.	0.00	0.01	0.00	0.00	0.01	0.00	0.02	0.01	0.00	0.00	0.02	0.01		
$\pi^0 e^+ \nu_e$ $M_{\rm bc}$ res.	2.62	1.27	3.77	1.17	1.97	2.09	0.01	0.01	0.01	0.05	0.08	0.01		
e^+ veto	0.26	−0.01	0.20	0.03	−0.14	0.07	0.02	0.09	0.02	0.12	−0.30	0.04		
FSR	0.26	0.48	0.47	0.68	0.65	0.49	0.25	0.46	0.55	0.64	0.60	0.41		
Model dep.	0.56	0.08	−0.08	0.76	0.08	0.28	0.35	−0.16	−0.28	−0.83	−1.51	−0.06		
Total	4.57	4.19	5.00	3.76	4.52	3.53	2.70	2.70	2.73	2.87	3.69	2.67		

uct of the CLEO-c hadronic branching-fraction analysis [26]. We combine the statistical and systematic uncertainties from that analysis for our uncertainty estimates.

We have assessed the uncertainties associated with the finding and identification efficiency for each of the signal hadrons. For the signal $K^\pm$ and $\pi^\pm$, the charged track-finding efficiency is already accounted in the tracking efficiency portion of the ν simulation uncertainty. They have, however, additional particle identification (PID) criteria associated with them, for which we assess a correction and uncertainty. For the signal π^0 and K^0_S we assess a correction and uncertainty for the reconstruction efficiencies of these particles. We evaluate each of these four uncertainties by first measuring a momentum dependent, and hence q^2 dependent, correction and fit the measurements with a linear parametrization. The best fit result is applied as a correction in the nominal fit. To evaluate the systematic uncertainty, we identify the largest systematic variation on the $\chi^2 = 1$ ellipse from the linear fit. The branching fractions are most affected by the largest variation in overall normalization, while the form factors (Sec. VII) are most affected by the largest variation in slope.

We have uncertainties associated with the electron identification efficiency and the rates for hadrons to misreconstruct as (fake) electrons. We vary the efficiency and fake rates used in the analysis of our MC samples (see Sec. IV B) according to the uncertainties from the data studies used to measure them, and refit the data to evaluate our sensitivity.

TABLE VI. Summary of full and partial branching-fraction systematic errors (%) associated with neutrino modeling in the MC for the $D^+ \to \pi^0 e^+ \nu_e$ and $D^+ \to \bar{K}^0 e^+ \nu_e$ signal decay modes. The sign represents the direction of change relative to the change in the $[0, 0.4)$ GeV$^2/c^4$ interval in each mode.

	$D^+ \to \pi^0 e^+ \nu_e$ q^2 interval (GeV$^2/c^4$)							$D^+ \to \bar{K}^0 e^+ \nu_e$ q^2 interval (GeV$^2/c^4$)						
ν Systematic	$[0, 0.4)$	$[0.4, 0.8)$	$[0.8, 1.2)$	$[1.2, 1.6)$	$[1.6, q^2_{\rm max}]$	All q^2		$[0, 0.4)$	$[0.4, 0.8)$	$[0.8, 1.2)$	$[1.2, 1.6)$	$[1.6, q^2_{\rm max}]$	All q^2	
Split-off showers	0.62	2.94	2.11	1.30	−1.68	1.14	0.17	0.37	0.21	−0.13	−1.36	0.18		
K^0_L showers	0.19	0.17	0.08	0.13	−0.83	−0.03	0.01	0.06	−0.08	−0.15	−0.46	−0.02		
K^0_L production	1.10	1.07	1.07	1.08	1.13	1.09	1.07	1.07	1.09	1.10	1.09	1.08		
Track efficiency	0.51	0.37	0.18	−0.14	0.13	0.24	0.62	0.57	0.70	0.66	0.39	0.62		
Track resolution	1.08	0.05	−0.09	−0.90	0.13	0.12	0.43	0.45	0.64	0.49	0.92	0.49		
Split-off rejection	1.66	1.08	0.68	1.45	−0.81	0.86	0.81	0.88	0.84	0.99	0.21	0.84		
Particle ID	0.09	−0.02	0.04	0.07	−0.03	0.03	0.01	0.02	0.00	0.01	0.08	0.01		
Shower resolution	0.00	−0.01	0.18	0.30	0.04	0.08	0.00	−0.02	0.03	−0.01	−0.09	0.00		
Fake tracks	0.77	0.71	0.70	0.71	0.71	0.72	0.72	0.70	0.69	0.69	0.70	0.71		
Total	2.54	3.41	2.57	2.53	2.45	1.96	1.71	1.75	1.82	1.84	2.18	1.74		

Modeling of $\pi^{\pm}$ and π^0 production—spectra and rates—in D decay significantly affects the background shape and rate for the signal cross feed background into the pion signal modes. The large effect results because a pion from the nonsignal D decay can be swapped in as the signal pion candidate. We measure the background pion spectra in data using the inclusive D decays on the ''other side'' of a fully reconstructed hadronically-decayed D ''tag,'' and correct the MC spectra accordingly. To be conservative in the associated systematic uncertainty, we take the full difference for results obtained using corrected and uncorrected spectra. In the signal $D^0 \to \pi^- e^+ \nu_e$ mode we also correct the cross feed background from $D^0 \to K^- e^+ \nu_e$ events that results from misidentifying a $K^{\pm}$ as a $\pi^{\pm}$. Once again the uncertainty estimate is taken as the difference of our measured rates obtained using the corrected and uncorrected fake rates.

For three of our signal modes, $D^0 \to \pi^- e^+ \nu_e$, $D^0 \to K^- e^+ \nu_e$, and $D^+ \to \pi^0 e^+ \nu_e$, we have systematic uncertainty associated with the additional $M_{\rm bc}$ resolution parameter. The statistical uncertainty already has a contribution from allowing this parameter to float. We estimate the contribution to the systematic uncertainty for each mode by increasing the value of that mode's resolution parameter by 1 standard deviation beyond the best fit result.

We must also account for any uncertainty associated with modeling event loss from the single electron veto because of secondary electrons from photon conversions and other processes. According to data studies (using the CLEO-c ''tagged'' samples, where one of the two D mesons from the $\psi(3770)$ is fully reconstructed), our MC simulation models the number of secondary electrons in our events accurately within the error of the study. The most likely potential source of uncertainty arises from mismodeling the rate for photon conversion within the detector material. For the uncertainty estimate we therefore vary this contribution over the range allowed by the maximum allowed uncertainty of our data study, about 8%.

For the systematic uncertainty associated with the FSR modeling, we take the difference between the KLOR and PHOTOS [27] predictions, with interference terms turned off in the latter. This simulates a change in the radiative branching fraction of up to 16% in the most extreme case. Because the majority of the correction results from the lack of the FSR interference terms between the charged hadron and electron, the systematic should be an overestimate of the FSR uncertainty from final or initial-state particles. This overestimate compensates for the unknown direct (structure-dependent) contributions.

The final systematic uncertainty we assess is the dependence on our modeling of the form factor input to our signal MC. We reweight each of our signal MC samples with a different form factor input, namely, ISGW2. The nominal form factor input to our signal MC is a BK parametrization [9] with parameters determined by lattice QCD [2]. The q^2 spectra of the latter differ markedly from those of ISGW2. We fit with the reweighted MC spectra and the difference to the nominal fit gives the systematic error associated with model dependence. The small uncertainties obtained in this study confirm our conclusion drawn from fitting the large MC sample.

VI. BRANCHING-FRACTION RESULTS

Combining the results of the fit and the systematic uncertainty estimates gives us the final efficiency-corrected yield measurement for each mode. From that yield (Y), we obtain the branching fraction $\mathcal{B} = Y/2N_{D\bar{D}}$, where $N_{D\bar{D}}$ is the number of neutral ($N_{D^0\bar{D}^0}$) or charged ($N_{D^+D^-}$) pairs in our sample. We obtain these numbers from an independent CLEO-c analysis [26] based on the comparison of events with one reconstructed D to events with both D decays reconstructed, in certain hadronic modes. For the same data set that we have used, that analysis finds $N_{D^0\bar{D}^0} = (1.031 \pm 0.016) \times 10^6$ and $N_{D^+D^-} = (0.819 \pm 0.013) \times 10^6$. Our fit yields, efficiencies and branching fractions for each mode, in each q^2 range, are presented in Table VII. The total branching fractions for each mode (also listed in Table VII) are

$$\mathcal{B}(D^0 \to \pi^- e^+ \nu_e) = 0.299(11)(9)\%, \tag{14}$$

$$\mathcal{B}(D^+ \to \pi^0 e^+ \nu_e) = 0.373(22)(13)\%, \tag{15}$$

$$\mathcal{B}(D^0 \to K^- e^+ \nu_e) = 3.56(3)(9)\%, \tag{16}$$

and

$$\mathcal{B}(D^+ \to \bar{K}^0 e^+ \nu_e) = 8.53(13)(23)\%. \tag{17}$$

The errors listed are statistical and systematic, respectively.

We also measure the branching-fraction and partial width ratios in each q^2 range. The full results are given in Table VII. To determine the partial width ratios we used the Particle Data Group lifetimes [4] $\tau_{D^0} = 410.3 \pm 1.5$ fs and $\tau_{D^+} = 1040 \pm 7$ fs. For the integrated q^2 ranges we find the ratios of branching fractions

$$R_0 \equiv \frac{\mathcal{B}(D^0 \to \pi^- e^+ \nu_e)}{\mathcal{B}(D^0 \to K^- e^+ \nu_e)} = 8.41(32)(13)\% \tag{18}$$

and

$$R_+ \equiv \frac{\mathcal{B}(D^+ \to \pi^0 e^+ \nu_e)}{\mathcal{B}(D^+ \to \bar{K}^0 e^+ \nu_e)} = 4.37(27)(12)\%. \tag{19}$$

The partial width ratios, which are expected to satisfy isospin relationships, are found to be

$$I_\pi \equiv \frac{\Gamma(D^0 \to \pi^- e^+ \nu_e)}{\Gamma(D^+ \to \pi^0 e^+ \nu_e)} = 2.03(14)(8) \tag{20}$$

and

TABLE VII. Summary of the efficiencies (ε) and efficiency-corrected yields for each q^2 interval and the corresponding partial branching fractions, the total branching fractions, the branching ratios, and the isospin ratios. In all cases the first errors are statistical and the second are systematic. For the $\bar{K}^0$ mode, the efficiency and yields correspond to the reconstructed $K^0_S \to \pi^+\pi^-$ mode, so do not include the initial production amplitude or $\pi^+\pi^-$ branching-fraction factors.

	q^2 interval (GeV^2/c^4)					
	<0.4	0.4–0.8	0.8–1.2	1.2–1.6	≥ 1.6	Total
			$D^0 \to \pi^- e^+ \nu_e$			
ε (%)	19.4	21.0	22.4	22.8	22.4	–
Yield	1452(113)(49)	1208(102)(35)	1242(99)(36)	906(85)(29)	1357(103)(46)	–
$\mathcal{B}(\pi^- e^+ \nu_e)(\%)$	0.070(5)(3)	0.059(5)(2)	0.060(5)(2)	0.044(4)(2)	0.066(5)(2)	0.299(11)(9)
			$D^+ \to \pi^0 e^+ \nu_e$			
ε (%)	7.5	8.0	7.9	7.2	5.7	–
Yield	1379(168)(59)	1584(180)(61)	1012(154)(48)	1028(158)(35)	1101(174)(47)	–
$\mathcal{B}(\pi^0 e^+ \nu_e)(\%)$	0.084(10)(4)	0.097(11)(4)	0.062(9)(3)	0.063(10)(2)	0.067(11)(3)	0.373(22)(13)
			$D^0 \to K^- e^+ \nu_e$			
ε (%)	19.2	20.5	20.0	18.3	13.9	–
Yield	29 701(441)(569)	21 600(377)(473)	14 032(304)(301)	7001(225)(178)	991(112)(20)	–
$\mathcal{B}(K^- e^+ \nu_e)(\%)$	1.441(21)(35)	1.048(18)(28)	0.681(15)(18)	0.340(11)(10)	0.048(5)(12)	3.557(33)(90)
			$D^+ \to \bar{K}^0 e^+ \nu_e$			
ε (%)	11.7	12.3	12.5	12.2	12.5	–
Yield	19 480(466)(417)	14 422(415)(306)	9009(327)(194)	4656(236)(107)	789(104)(26)	–
$\mathcal{B}(\bar{K}^0 e^+ \nu_e)(\%)$	3.436(82)(93)	2.544(73)(69)	1.589(58)(44)	0.821(42)(24)	0.139(18)(5)	8.53(13)(23)
			Branching ratios and isospin ratios			
$R_0(\%)$	4.89(39)(12)	5.59(48)(12)	8.85(74)(15)	12.9(13)(2)	137(19)(3)	8.41(32)(13)
$R_+(\%)$	2.45(31)(9)	3.80(45)(13)	3.89(61)(17)	7.6(12)(2)	48(10)(2)	4.37(27)(12)
I_π	2.12(31)(9)	1.54(22)(7)	2.47(43)(13)	1.78(32)(7)	2.48(45)(13)	2.03(14)(8)
I_K	1.06(3)(3)	1.04(4)(3)	1.09(5)(3)	1.05(6)(4)	0.88(15)(3)	1.06(2)(3)

$$I_K \equiv \frac{\Gamma(D^0 \to K^- e^+ \nu_e)}{\Gamma(D^+ \to \bar{K}^0 e^+ \nu_e)} = 1.06(2)(3). \qquad (21)$$

We expect $I_\pi = 2$ and $I_K = 1$, hence the measured partial width ratios satisfy isospin symmetry within our experimental precision.

VII. FORM FACTORS

For each of our four signal decay modes we have obtained partial branching-fraction results in five q^2 ranges. To extract information about the form factors we use the relationship

$$\mathcal{B}_i = \frac{G_F^2 |V_{cq}|^2}{24\pi^3 \Gamma_D} \int_{q^2_{\min}(i)}^{q^2_{\max}(i)} p^3 |f_+(q^2)|^2 dq^2 \qquad (22)$$

to relate the form factor $f_+(q^2)$ to the partial branching fraction $\mathcal{B}$ in a particular q^2 range. In this expression, Γ_D is the total decay width of the parent D meson, and i denotes the particular q^2 interval. A specific functional form is chosen for $f_+(q^2)$ (see Sec. II) and the parameter values are determined via a χ^2 fit to the five measured $\mathcal{B}_i$. In order to account for the correlations between the branching fractions in each q^2 range we minimize the expression

$$\chi^2 = \sum_{ij} (\mathcal{B}_i - y_i) C^{-1}_{ij} (\mathcal{B}_j - y_j), \qquad (23)$$

where y_i is the fit prediction for the branching fraction in the ith q^2 interval, and C^{-1}_{ij} is the inverse of the covariance matrix. The integration in each bin is performed numerically on each fit iteration using the trapezoidal rule.

The systematic uncertainties on the form factor parameters are evaluated using the same method as for the branching-fraction analysis. We take the set of branching fractions that result from the branching-fraction fit for each systematic uncertainty, then redo the fit for the form factors. The difference in these fit parameters from the nominal results is taken as the estimate of the systematic uncertainty. The list of systematic uncertainties evaluated is the same as for the branching-fraction analysis (see Sec. V).

Fitting with the full covariance matrix that includes both statistical and systematic uncertainties and correlations (see Appendix B) yields almost identical central values and total errors.

We evaluate the form factor shape using the functional form given by the series parametrization as described in Sec. II. For comparative purposes we also provide results based on the two pole models described in Sec. II. For the series model we perform fits using both the first two and the first three expansion parameters a_k. This tests both our sensitivity to the number of parameters in the expansion and the convergence of the series. We express our results in

TABLE VIII. Summary of form factor results for the series parametrization and pole-model fits. Correlation coefficients for the total uncertainty between variables in any two (three) preceding columns are given by ρ (ρ_{ij}). The first errors are statistical and the second are systematic. The values for the $\pi^0 e^+ \nu_e$ mode are isospin corrected. For the series parameters (a_i) we have assumed $|V_{cs}| = 0.976$ and $|V_{cd}| = 0.224$.

Series Parametrization—Three-Parameter Fits										
Decay	a_0	a_1	a_2	ρ_{01}	ρ_{02}	ρ_{12}	$\lvert V_{cq}\rvert f_+(0)$	$1 + 1/\beta - \delta$	ρ	χ^2/d.o.f
$\pi^- e^+ \nu_e$	0.044(2)(1)	−0.18(7)(2)	−0.03(35)(12)	0.81	0.71	0.96	0.140(7)(3)	1.30(37)(12)	−0.85	2.0/2
$\pi^0 e^+ \nu_e$	0.044(3)(1)	−0.23(11)(2)	−0.60(57)(15)	0.80	0.67	0.95	0.138(11)(4)	1.58(60)(13)	−0.86	2.8/2
$K^- e^+ \nu_e$	0.0234(3)(3)	−0.009(21)(7)	0.52(28)(6)	0.62	0.56	0.96	0.747(9)(9)	0.62(13)(4)	−0.62	0.2/2
$\bar{K}^0 e^+ \nu_e$	0.0224(4)(3)	0.009(32)(7)	0.76(42)(8)	0.72	0.64	0.96	0.733(14)(11)	0.51(20)(4)	−0.72	1.7/2

Series Parametrization—Two-Parameter Fits							
Decay	a_0	a_1	ρ	$\lvert V_{cq}\rvert f_+(0)$	$1 + 1/\beta - \delta$	ρ	χ^2/d.o.f
$\pi^- e^+ \nu_e$	0.044(2)(1)	−0.173(19)(7)	0.66	0.140(5)(3)	1.27(11)(4)	−0.80	2.0/3
$\pi^0 e^+ \nu_e$	0.046(2)(1)	−0.124(30)(9)	0.69	0.147(7)(4)	1.01(16)(5)	−0.78	4.0/3
$K^- e^+ \nu_e$	0.0230(2)(3)	−0.047(6)(3)	0.34	0.734(6)(9)	0.86(4)(2)	−0.43	3.8/3
$\bar{K}^0 e^+ \nu_e$	0.0218(3)(3)	−0.046(9)(4)	0.53	0.713(9)(11)	0.87(6)(3)	−0.60	4.9/3

	Simple Pole-Model Fits				Modified Pole-Model Fits			
Decay	$\lvert V_{cq}\rvert f_+(0)$	m_{pole} (GeV/c^2)	ρ	χ^2/d.o.f	$\lvert V_{cq}\rvert f_+(0)$	α	ρ	χ^2/d.o.f
$\pi^- e^+ \nu_e$	0.146(4)(2)	1.87(3)(1)	0.63	3.11/3	0.142(4)(2)	0.37(8)(3)	−0.75	2.1/3
$\pi^0 e^+ \nu_e$	0.149(6)(3)	1.97(7)(2)	0.65	4.42/3	0.147(7)(4)	0.14(16)(4)	−0.75	4.07/3
$K^- e^+ \nu_e$	0.735(5)(9)	1.97(3)(1)	0.36	2.67/3	0.732(6)(9)	0.21(5)(3)	−0.42	4.32/3
$\bar{K}^0 e^+ \nu_e$	0.710(8)(10)	1.96(4)(2)	0.53	4.1/3	0.708(9)(10)	0.22(8)(3)	−0.59	5.3/3

terms of the physical observables, the intercept $|V_{cq}|f_+(0)$ and $1 + 1/\beta - \delta$, as well as giving the expansion parameters. In the simple pole model we fit for the intercept and the pole mass m_{pole}, while in the modified pole model we fit for the intercept and the shape parameter α, which summarizes the effective pole contribution. The results for all modes are summarized in Table VIII. Comparisons of the four fits, for each of the four modes, are shown in Fig. 3. To allow systematic differences to be viewed clearly between the various parametrizations, we normalize the data and all fit results to the result of the three-parameter series fit in each q^2 interval.

For the series expansion, comparison of the two-parameter and three-parameter fits shows that our kaon data prefer a nonzero quadratic z term. The probability of χ^2 improves from 29% (22%) to 89% (44%) going from two to three terms in the series for the $K^-(K^0)$ fit. The pion measurements currently lack sensitivity to probe this term, and two- and three-parameter fits yield similar results for the first two parameters. Since a quadratic term appears to be preferred for the kaons, however, we include that term in our series fits to the pion data to improve the probability that our shape uncertainties bracket the true form factor shape. While the central value for a_2 is an order of magnitude larger than the other terms, we stress that regions of parameter space with a_2 of similar magnitude to a_0 and a_1 fall well within the 90% probability hypercontour for the fit, so no strong statements can be made about the size of a_2 or about the convergence (or potential lack thereof) of the series from these data.

For the pole models we observe that the parametrizations can provide a shape that describes our data adequately, but only with parameter values that do not support their physical basis. Although the fits give quite reasonable χ^2 values (see Table VIII), the pole masses do not agree with the $M_{D_s^*}$ (M_{D^*}) masses expected for the kaon (pion) modes by over 3σ for the most precise fits. Furthermore, the probability of χ^2 improves noticeably

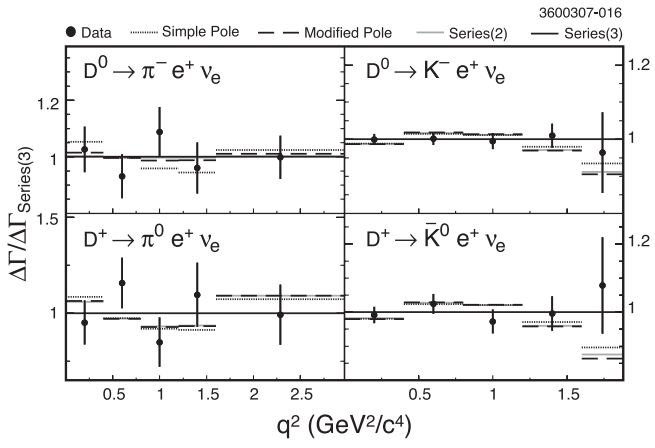

FIG. 3. Form factor fit comparison for all modes. All data (points) and fits (histograms) are normalized to the relevant three-parameter series fit result [Series (3), line at 1]. The simple pole, modified pole, and two-parameter series fit [Series (2)] are shown by triple-dot-dash, dashed, and solid histograms, respectively.

for our three parameter z expansion fit relative to these pole fits. The $1 + 1/\beta - \delta$ results from the $D^0 \to K^- e^+ \nu_e$ series expansion fit are over 3σ from the value of ~ 2 necessary for physical validity of the BK parametrization, while those derived from our α values for the kaon modes are tens of σ away.

VIII. EXTRACTION OF $|V_{cs}|$ AND $|V_{cd}|$

We extract $|V_{cd}|$ and $|V_{cs}|$ by combining our $|V_{cq}|f_+(0)$ results from the three-parameter series expansion fits with the unquenched LQCD results [2] $f_+^{(D\to\pi)}(0) = 0.64(3)(6)$ and $f_+^{(D\to K)}(0) = 0.73(3)(7)$. For the $D^0 \to \pi^-$ and $D^+ \to \pi^0$ modes we find $|V_{cd}| = 0.218 \pm 0.011 \pm 0.005 \pm 0.023$ and $|V_{cd}| = 0.216 \pm 0.017 \pm 0.006 \pm 0.023$, respectively. For the $D^0 \to K^-$ and $D^+ \to \bar{K}^0$ modes, we find $|V_{cs}| = 1.023 \pm 0.013 \pm 0.013 \pm 0.107$ and $|V_{cs}| = 1.004 \pm 0.020 \pm 0.015 \pm 0.105$. Averaging the D^0 and D^+ results (taking into account correlated and uncorrelated uncertainties) we find

$$|V_{cd}| = 0.217 \pm 0.009 \pm 0.004 \pm 0.023 \tag{24}$$

and

$$|V_{cs}| = 1.015 \pm 0.010 \pm 0.011 \pm 0.106. \tag{25}$$

The uncertainties, statistical, systematic, and theoretical, respectively, are dominated by the discretization uncertainty in the LQCD charm quark action, which should be improved in the near future for the Fermilab action, or greatly reduced through the use of other actions.

We can also extract the ratio $|V_{cd}|/|V_{cs}|$ from the ratio of our measured form factors. From the z expansion fits to our D^0 data, we obtain $|V_{cd}|f_+^{(D\to\pi)}(0)/|V_{cs}|f_+^{(D\to K)}(0) = 0.187 \pm 0.010 \pm 0.003$, while from our $D^\pm$ data we obtain $|V_{cd}|f_+^{(D\to\pi)}(0)/|V_{cs}|f_+^{(D\to K)}(0) = 0.188 \pm 0.015 \pm 0.004$. The errors are statistical and systematic, respectively, and all correlations have been taken into account. Averaging, again with correlated uncertainties accounted for, we obtain

$$\frac{|V_{cd}|f_+^{(D\to\pi)}(0)}{|V_{cs}|f_+^{(D\to K)}(0)} = 0.188 \pm 0.008 \pm 0.002. \tag{26}$$

We can combine this result with calculations of $f(0)^{(D\to\pi)}/f(0)^{(D\to K)}$ to obtain the ratio of CKM elements. A recent light cone sum rules (LCSR) calculation, for example, obtains [28] $f_+^{(D\to\pi)}(0)/f_+^{(D\to K)}(0) = 0.84 \pm 0.04$, which implies

$$\frac{|V_{cd}|}{|V_{cs}|} = 0.223 \pm 0.010_{\text{stat}} \pm 0.003_{\text{syst}} \pm 0.011_{\text{LCSR}}. \tag{27}$$

IX. SUMMARY

In summary, we have measured branching fractions and branching-fraction ratios for four semileptonic D decay modes in five q^2 bins. The branching-fraction results are the most precise measured to date and agree well with world averages [4]. Our modified pole α parameter results agree within 1.3σ with previous determinations by CLEO III [10], FOCUS [11], and $Ke\nu$ results from Belle [12], but show over 3σ disagreement with Belle $K\mu\nu$ results and LQCD fits. The α parameters obtained with our individual $Ke\nu$ results are separated from the recent BABAR result [13] by about 2.5σ. For $Ke\nu$, the z expansion parameters found by BABAR and this measurement agree to better than 2σ, with the precise level depending on the correlation coefficient for the BABAR r_1 and r_2 parameters. The discrepancy with LQCD is difficult to quantify because the covariance matrix for the LQCD form factors is lost during the chiral extrapolation procedure for the published analysis [2]. We have made the most precise CKM determinations from D semileptonic decays to date, and the results agree very well with neutrino based determinations of $|V_{cd}|$ and charmed-tagged W decay measurements of $|V_{cs}|$ [4]. Overall, these measurements represent a marked improvement in our knowledge of D semileptonic decay.

ACKNOWLEDGMENTS

We gratefully acknowledge the effort of the CESR staff in providing us with excellent luminosity and running conditions. D. Cronin-Hennessy and A. Ryd thank the A. P. Sloan Foundation. This work was supported by the National Science Foundation, the U.S. Department of Energy, and the Natural Sciences and Engineering Research Council of Canada.

APPENDIX A: THE z EXPANSION: DETAILED FORMS AND ALTERNATE RESULTS

The standard choice for the outer function $\phi(t, t_0)$ in the z expansion for $f_+(q^2)$ [Eq. (12)] arises from considerations of unitarity. From a perturbative operator product expansion (OPE) calculation, one can show [7,15,29] that the choice

$$\phi(t, t_0) = \alpha(\sqrt{t_+ - t} + \sqrt{t_+ - t_0})\frac{t_+ - t}{(t_+ - t_0)^{1/4}} \times \frac{(\sqrt{t_+ - t} + \sqrt{t_+ - t_-})^{3/2}}{(\sqrt{t_+ - t} + \sqrt{t_+})^5} \tag{A1}$$

leads to a constraint on the coefficients

$$\sum_{k=0}^{n_a} a_k^2 \le 1, \tag{A2}$$

TABLE IX. The fit results for the three parameter z expansion fit for both $t_0 = 0$ and $t_0 = t_+(1 - \sqrt{1 - t_-/t_+})$. The fit results are also presented in terms of the ratios $r_i = a_i/a_0$ for $i = 1, 2$.

		a_0	a_1	a_2	ρ_{01}	ρ_{02}	ρ_{12}
$t_0 = 0$	$\pi^- e^+ \nu_e$	0.044(2)(1)	−0.18(7)(2)	−0.03(35)(12)	0.81	0.71	0.96
	$\pi^0 e^+ \nu_e$	0.044(3)(1)	−0.23(11)(2)	−0.60(57)(15)	0.80	0.67	0.95
	$K^- e^+ \nu_e$	0.0234(3)(3)	−0.009(21)(7)	0.52(28)(6)	0.62	0.56	0.96
	$\bar{K}^0 e^+ \nu_e$	0.0224(4)(3)	0.009(32)(7)	0.76(42)(8)	0.72	0.64	0.96
		a_0	r_1	r_2	ρ_{01}	ρ_{02}	ρ_{12}
$t_0 = 0$	$\pi^- e^+ \nu_e$	0.044(2)(1)	−4.1(1.7)(0.6)	−0.7(8.0)(2.9)	0.85	0.71	0.95
	$\pi^0 e^+ \nu_e$	0.044(3)(1)	−5.3(2.8)(0.5)	−14(14)(3)	0.85	0.71	0.95
	$K^- e^+ \nu_e$	0.0234(3)(3)	−0.4(9)(3)	22(12)(2)	0.62	0.54	0.95
	$\bar{K}^0 e^+ \nu_e$	0.0224(4)(3)	0.4(1.4)(3)	34(18)(4)	0.72	0.61	0.96
		a_0	a_1	a_2	ρ_{01}	ρ_{02}	ρ_{12}
$t_0 = t_+(1 - \sqrt{1 - t_-/t_+})$	$\pi^- e^+ \nu_e$	0.072(2)(1)	−0.15(5)(2)	−0.09(35)(13)	−0.48	0.21	−0.94
	$\pi^0 e^+ \nu_e$	0.065(4)(1)	−0.01(10)(2)	−0.63(57)(14)	−0.65	0.41	−0.95
	$K^- e^+ \nu_e$	0.0252(2)(3)	−0.062(10)(2)	0.52(28)(6)	−0.14	−0.24	−0.79
	$\bar{K}^0 e^+ \nu_e$	0.0239(3)(3)	−0.067(15)(4)	0.76(42)(9)	−0.08	−0.28	−0.82
		a_0	r_1	r_2	ρ_{01}	ρ_{02}	ρ_{12}
$t_0 = t_+(1 - \sqrt{1 - t_-/t_+})$	$\pi^- e^+ \nu_e$	0.072(2)(1)	−2.1(7)(3)	−1.2(4.8)(1.7)	−0.41	0.22	−0.96
	$\pi^0 e^+ \nu_e$	0.065(4)(1)	−0.2(1.5)(4)	−9.8(9.1)(2.1)	−0.64	0.47	−0.97
	$K^- e^+ \nu_e$	0.0252(2)(3)	−2.4(4)(1)	21(11)(2)	−0.05	−0.27	−0.81
	$\bar{K}^0 e^+ \nu_e$	0.0239(3)(3)	−2.8(6)(2)	32(18)(4)	0.004	−0.31	−0.84

for any choice of n_a. The bound corresponds to forbidding the production rate of $D\pi$ states by the relevant current to exceed the inclusive production rate, which can be calculated within the OPE. To leading order, the coefficient α is given by

$$\alpha = \sqrt{\frac{\pi m_c^2}{3}}. \tag{A3}$$

Numerically, we have taken the charm quark mass to be $m_c = 1.2$ GeV. Note however that this analysis is subject to $\mathcal{O}(1/M)$ corrections, where M is the heavy quark mass, so the validity of the constraint (A2) is unclear for the D system.

The choice of the parameter t_0 within the z expansion provides a potential source of ambiguity when comparing experimental results. In our fits, we have, for simplicity, chosen $t_0 = 0$ in our form factor fits utilizing the z expansion. Another common choice for t_0 is that which minimizes the maximal value of the mapping $z(q^2)$ over the entire physical range. The value $t_0 = t_+(1 - \sqrt{1 - t_-/t_+})$, where $t_\pm = m_D \pm m_{K,\pi}$ accomplishes this minimization. The best fit a_i values for our three-parameter fit using this alternate value for t_0 are presented in Table IX. The values for $|V_{cq}|f_+(0)$ $(q = s, d)$ that we find in these fits are identical, within the precision we are quoting, to those presented in Table VIII.

Finally, some experimental results for the z expansion are presented in terms of the ratios $r_i = a_i/a_0$ for $i > 0$. To allow straightforward comparison, we also quote our results in this form in Table IX.

APPENDIX B: CORRELATION MATRICES

To allow complete external use of the partial branching fractions presented in this paper, we present the statistical and systematic uncertainty correlation matrices. These matrices will allow, for example, for simultaneous fits of these results with other experimental results to obtain form factor parameters. The statistical correlation matrix (Table X) is derived from the 20×20 covariance matrix produced in our fitting procedure.

To obtain the systematic correlation matrix (Table XI), we create a separate covariance matrix from the correlated motions of all 20 yields in each individual systematic study. We then sum the resulting matrices to obtain the total systematic covariance matrix. In the absence of correlations, this procedure would reduce to adding the systematic contributions for a given measurement in quadrature. In producing the covariance matrix for the form factor systematic uncertainty, we assume that the two pion modes are fully correlated and similarly for the two kaon modes, but treat the pion and kaon uncertainties as uncorrelated. For the $N_{D^+D^-}$ and $N_{D^0\bar{D}^0}$ uncertainties, we take into account the 39% correlation in those yields.

TABLE X. The statistical correlation matrix obtained from the simultaneous fit to the data (see Sec. IV B). The lines indicate the mode boundaries. The modes are labeled by their final state hadron. Within each submode, the five q^2 intervals are ordered from lowest to highest.

	π^-					π^0					K^-					$\bar{K}^0$				
	1.000	−0.047	0.034	0.025	0.030	−0.002	0.002	0.003	0.004	0.002	−0.059	0.003	0.002	0.002	0.000	−0.010	0.006	0.009	0.010	0.006
		1.000	−0.045	0.034	0.035	0.001	−0.005	0.003	0.006	0.004	−0.007	−0.026	0.004	0.003	0.000	0.002	−0.014	0.011	0.014	0.009
π^-			1.000	−0.044	0.034	0.001	0.002	−0.008	0.004	0.006	0.000	−0.009	−0.013	0.001	0.000	0.004	0.003	−0.019	0.011	0.010
				1.000	−0.016	0.001	0.002	0.004	−0.022	0.006	−0.001	0.000	−0.009	−0.011	0.001	0.002	0.007	−0.003	−0.038	−0.001
					1.000	−0.001	−0.001	−0.001	0.007	−0.115	−0.002	−0.002	−0.003	−0.021	−0.030	−0.004	−0.002	−0.004	−0.022	−0.053
						1.000	−0.089	0.033	0.017	0.018	0.000	0.000	0.000	0.000	−0.001	−0.013	0.006	0.005	0.004	0.001
							1.000	−0.094	0.032	0.023	0.001	−0.001	0.000	0.001	0.000	−0.006	−0.010	0.006	0.004	0.001
π^0								1.000	−0.090	0.032	0.001	0.001	−0.002	0.001	0.000	0.004	−0.006	−0.016	0.002	0.002
									1.000	−0.069	0.001	0.001	0.000	−0.004	−0.002	0.002	0.004	−0.013	−0.029	−0.005
										1.000	0.001	0.001	0.000	−0.005	−0.012	−0.002	−0.004	−0.003	−0.028	−0.051
											1.000	−0.064	0.023	0.017	0.012	−0.033	0.006	0.005	0.005	0.002
												1.000	−0.070	0.021	0.011	0.002	−0.019	0.006	0.007	0.003
K^-													1.000	−0.071	0.013	0.007	0.005	−0.021	0.001	0.002
														1.000	−0.094	0.005	0.007	0.000	−0.040	−0.016
															1.000	0.000	0.000	−0.001	−0.019	−0.062
																1.000	−0.068	0.031	0.019	0.007
																	1.000	−0.060	0.027	0.009
$\bar{K}^0$																		1.000	−0.068	0.011
																			1.000	−0.098
																				1.000

TABLE XI. The total systematic correlation matrix for the 20 measured mode/q^2 intervals (see Sec. V). The lines indicate the mode boundaries. The modes are labeled by their final state hadron. Within each mode, the five q^2 intervals are ordered from lowest to highest.

	π^-					π^0					K^-					$\bar{K}^0$				
	1.00	0.73	0.64	0.59	0.51	0.45	0.29	0.13	0.28	0.06	0.75	0.59	0.56	0.53	0.59	0.34	0.27	0.22	0.26	0.26
		1.00	0.87	0.81	0.56	0.13	0.33	0.21	0.34	−0.04	0.75	0.74	0.74	0.70	0.63	0.28	0.32	0.32	0.26	0.13
π^-			1.00	0.94	0.46	0.23	0.55	0.34	0.39	−0.20	0.79	0.86	0.86	0.85	0.64	0.25	0.32	0.28	0.19	−0.10
				1.00	0.46	0.19	0.61	0.38	0.44	−0.21	0.77	0.89	0.89	0.91	0.65	0.23	0.30	0.27	0.17	−0.11
					1.00	0.05	0.14	0.08	0.10	0.24	0.57	0.52	0.52	0.50	0.56	0.20	0.18	0.19	0.22	0.37
						1.00	0.70	0.77	0.68	0.41	0.35	0.27	0.24	0.22	0.20	0.56	0.53	0.47	0.49	0.31
							1.00	0.83	0.75	0.01	0.46	0.58	0.57	0.62	0.32	0.56	0.62	0.56	0.46	0.07
π^0								1.00	0.71	0.31	0.28	0.37	0.36	0.39	0.19	0.40	0.45	0.42	0.34	0.07
									1.00	0.36	0.44	0.49	0.48	0.48	0.31	0.64	0.70	0.68	0.63	0.32
										1.00	−0.04	−0.15	−0.14	−0.19	0.03	0.29	0.24	0.28	0.36	0.57
											1.00	0.93	0.92	0.86	0.75	0.40	0.39	0.35	0.30	0.11
												1.00	1.00	0.98	0.81	0.33	0.40	0.38	0.31	0.03
K^-													1.00	0.98	0.82	0.33	0.40	0.38	0.31	0.05
														1.00	0.82	0.28	0.37	0.35	0.28	0.02
															1.00	0.19	0.30	0.30	0.38	0.37
																1.00	0.96	0.94	0.88	0.62
																	1.00	0.99	0.94	0.63
$\bar{K}^0$																		1.00	0.96	0.67
																			1.00	0.80
																				1.00

[1] M. Kobayashi and T. Maskawa, Prog. Theor. Phys. **49**, 652 (1973).
[2] C. Aubin *et al.*, Phys. Rev. Lett. **94**, 011601 (2005).
[3] R. A. Briere *et al.* (CESR-c and CLEO-c Taskforces, CLEO-c Collaboration), Cornell University LEPP Report No. CLNS 01/1742, 2001 (unpublished).
[4] W. M. Yao *et al.*, J. Phys. G **33**, 1 (2006).
[5] D. Cronin-Hennessy *et al.* (CLEO Collaboration), arXiv: 0712.0998 [Phys. Rev. Lett. (to be published)].
[6] G. S. Huang *et al.* (CLEO Collaboration), Phys. Rev. Lett. **95**, 181801 (2005); T. E. Coan *et al.*, Phys. Rev. Lett. **95**, 181802 (2005).
[7] C. G. Boyd, B. Grinstein, and R. F. Lebed, Phys. Rev. Lett. **74**, 4603 (1995).
[8] R. J. Hill, arXiv:hep-ph/0606023.
[9] D. Becirevic and A. B. Kaidalov, Phys. Lett. B **478**, 417 (2000).
[10] G. S. Huang *et al.* (CLEO Collaboration), Phys. Rev. Lett. **94**, 011802 (2005).
[11] J. M. Link *et al.* (FOCUS Collaboration), Phys. Lett. B **607**, 233 (2005).
[12] L. Widhalm *et al.* (Belle Collaboration), Phys. Rev. Lett. **97**, 061804 (2006).
[13] B. Aubert *et al.* (BABAR Collaboration), Phys. Rev. D **76**, 052005 (2007).
[14] E. Gulez, A. Gray, M. Wingate, C. T. H. Davies, G. P. Lepage, and J. Shigemitsu, Phys. Rev. D **73**, 074502 (2006).
[15] C. G. Boyd and M. J. Savage, Phys. Rev. D **56**, 303 (1997).
[16] C. M. Arnesen, B. Grinstein, I. Z. Rothstein, and I. W. Stewart, Phys. Rev. Lett. **95**, 071802 (2005).
[17] T. Becher and R. J. Hill, Phys. Lett. B **633**, 61 (2006).
[18] S. B. Athar *et al.* (CLEO Collaboration), Phys. Rev. D **68**, 072003 (2003).
[19] G. Viehhauser, Nucl. Instrum. Methods Phys. Res., Sect. A **462**, 146 (2001); D. Peterson *et al.*, Nucl. Instrum. Methods Phys. Res., Sect. A **478**, 142 (2002).
[20] M. Artuso *et al.* (CLEO Collaboration), Nucl. Instrum. Methods Phys. Res., Sect. A **554**, 147 (2005).
[21] R. Barlow and C. Beeston, Comput. Phys. Commun. **77**, 219 (1993).
[22] D. J. Lange, Nucl. Instrum. Methods Phys. Res., Sect. A **462**, 152 (2001).
[23] R. Brun *et al.*, CERN Report No. DD/EE/84-1, 1987.
[24] T. C. Andre, Ann. Phys. (N.Y.) **322**, 2518 (2007); T. Alexopoulos *et al.*, Phys. Rev. D **71**, 012001 (2005).
[25] D. Scora and N. Isgur, Phys. Rev. D **52**, 2783 (1995).
[26] S. Dobbs *et al.* (CLEO Collaboration), Phys. Rev. D **76**, 112001 (2007).
[27] Using PHOTOS v2.0, E. Barberio and Z. Was, Comput. Phys. Commun. **79**, 291 (1994).
[28] P. Ball, Phys. Lett. B **641**, 50 (2006).
[29] C. Bourrely, B. Machet, and E. de Rafael, Nucl. Phys. **B189**, 157 (1981).